Published in final edited form as:
Traffic. 2009 September ; 10(9): 1318–1336. doi:10.1111/j.1600-0854.2009.00955.x.

ESCRT-I function is required for Tyrp1 transport from early endosomes to the melanosome limiting membrane

Steven T. Truschel[1,5], **Sabrina Simoes**[2,3,5], **Subba Rao Gangi Setty**[1], **Dawn C. Harper**[1], **Danièle Tenza**[2,3], **Penelope C. Thomas**[1], **Kathryn E. Herman**[1], **Sara D. Sackett**[1], **David C. Cowan**[1], **Alexander C. Theos**[1,4], **Graça Raposo**[2,3], and **Michael S. Marks**[1,*]

[1]Department of Pathology and Laboratory Medicine, University of Pennsylvania, Philadelphia, PA, 19104

[2]Institut Curie, Centre de Recherche, Paris, F-75248, France

[3]Centre National de la Recherche Scientifique, Unité Mixte de Recherche 144, Paris F-75248, France

[4]Department of Human Science, School of Nursing and Health Studies, Georgetown University, Washington, DC, 20057

Abstract

Melanosomes are lysosome-related organelles that coexist with lysosomes within melanocytes. The pathways by which melanosomal proteins are diverted from endocytic organelles toward melanosomes are incompletely defined. In melanocytes from mouse models of Hermansky-Pudlak syndrome (HPS) that lack BLOC-1, melanosomal proteins such as Tyrp1 accumulate in early endosomes. Whether this accumulation represents an anomalous pathway or an arrested normal intermediate in melanosome protein trafficking is not clear. Here we show that early endosomes are requisite intermediates in the trafficking of Tyrp1 from the Golgi to late stage melanosomes in normal melanocytic cells. Kinetic analyses show that very little newly synthesized Tyrp1 traverses the cell surface and that internalized Tyrp1 is inefficiently sorted to melanosomes. Nevertheless, nearly all Tyrp1 traverses early endosomes since it becomes trapped within enlarged, modified endosomes upon overexpression of Hrs. Although Tyrp1 localization is not affected by Hrs depletion, depletion of the ESCRT-I component, Tsg101, or inhibition of ESCRT function by dominant negative approaches results in a dramatic redistribution of Tyrp1 to aberrant endosomal membranes that are largely distinct from those harboring traditional ESCRT-dependent, ubiquitylated cargoes such as MART-1. The lysosomal protein content of some of these membranes and the lack of Tyrp1 recycling to the plasma membrane in Tsg101-depleted cells suggests that ESCRT-I functions downstream of BLOC-1. Our data delineate a novel pathway for Tyrp1 trafficking and illustrate a requirement for ESCRT-I function in controlling protein sorting from vacuolar endosomes to the limiting membrane of a lysosome-related organelle.

Keywords

melanosome; tyrosinase-related protein-1; early endosome; ESCRT; Tsg101

[*]To whom correspondence should be addressed: Michael S. Marks, Dept. of Pathology & Lab. Medicine, University of Pennsylvania, 513 Stellar Chance Labs/ 6100, 422 Curie Blvd., Philadelphia, PA 19104-6100, Tel: 215-898-3204, FAX: 215-573-4345, marksm@mail.med.upenn.edu.
[5]These authors contributed equally to this work.

Lysosome-related organelles (LRO) are a class of cell type-specific organelles that share features with lysosomes and other late endocytic organelles including a low intralumenal pH and the presence of resident lysosomal hydrolases and membrane proteins (1,2). Some LRO, such as cytolytic granules of T lymphocytes and natural killer cells, appear to be modified lysosomes with added functions while other LRO, such as melanosomes, coexist with lysosomes as separate organelles. The mechanisms and pathways by which components of the latter class of LRO are segregated from those of classical late endosomes and lysosomes are only beginning to be understood.

Melanosomes are LROs that function in the synthesis, storage and secretion of melanins in melanocytes and retinal pigment epithelia and provide an excellent model system for studying LRO biogenesis (3). Melanosomes develop through a series of four morphologically-defined stages that are enriched in a specific set of protein components (4,5). Stage I and II melanosomes are characterized by intralumenal fibrils, composed largely of the fibrillogenic protein Pmel17, but lack melanogenic enzymes such as tyrosinase and tyrosinase-related proteins. Melanin is synthesized and accumulates on the fibrils in melanosome stages III and IV as a consequence of the delivery of melanogenic enzymes to preformed stage II melanosomes. The pathways by which these enzymes are delivered are not yet clearly delineated.

Early endosomes play a special role in melanocytes, serving as intermediates for cargo bound both for lysosomes and melanosomes of different stages. For example, stage I melanosomes correspond functionally and morphologically to vacuolar domains of early endosomes, and serve as the site in which Pmel17 fibril formation is initiated (5). We have demonstrated previously that the melanosome-specific proteins Pmel17 and tyrosinase are both differentially sorted from early endosomes to stage II and III melanosomes, respectively. Tyrosinase is sorted to stage III melanosomes from tubular extensions of early endosomes, the buds of which are frequently enriched in the adaptor protein AP-3 (6). Accordingly, AP-3 deficiency in a subset of patients or mouse models of Hermansky-Pudlak Syndrome (HPS) results in missorting of a large cohort of tyrosinase to late endosomes (6,7). Pmel17 within early endosomes, like the melanocyte-specific protein MART-1 (8) and ubiquitylated lysosomal cargo in other cell types (9), becomes incorporated onto ILVs within vacuolar domains (5). Cleavage of Pmel17 within these organelles, which occurs concomitant with sequestration on ILVs, initiates formation of fibrils that eventually organize into fibrillar sheets within stage II melanosomes (10). While the incorporation of MART-1 (11) and several lysosomal cargoes onto ILVs requires ubiquitylation of the cytoplasmic domains and recognition of the ubiquitin moiety by components of the ESCRT pathway (for review see 12-14), Pmel17 sorting to ILVs does not require ubiquitylation, is insensitive to depletion of the ESCRT-0 component Hrs or to dominant negative disruption of ESCRT activity, and requires a lumenal determinant (15). Thus, melanosomal proteins like tyrosinase and Pmel17 are sorted from MART-1 and conventional late endocytic proteins within early endosomes by diverse mechanisms of spatial segregation mediated by cytoplasmic machinery and by lumenal interactions.

Whereas tyrosinase distribution is dramatically altered in AP-3-deficient melanocytes, the distribution of another mature melanosome resident, tyrosinase-related protein 1 (Tyrp1), is only mildly affected, with a modest increase in cell surface expression (16,17) but no obvious effect on intracellular distribution (7,18). Tyrp1 (also called TRP1 or GP75) shares 43% homology with tyrosinase (19,20), and has been proposed to stabilize tyrosinase on the melanosomal membrane (21) and to favor the accumulation of black melanin intermediates (22). At steady state, Tyrp1 resides predominantly in the limiting membrane of late stage (III/IV) melanosomes with a small cohort found in tubulovesicular structures near melanosomes or the Golgi (5,18) in MNT-1 melanoma and mouse melanocytes. The

interaction of newly-synthesized Tyrp1 with the PDZ-containing protein GIPC in the juxtanuclear Golgi region suggested that Tyrp1 might be sorted directly from the TGN to melanosomes (23), consistent with reconstitution of AP-1-dependent vesicular export of Tyrp1 from enriched Golgi membranes in vitro (24). However, other data support a pathway in which early endosomes serve as an intermediate in Tyrp1 trafficking. Like tyrosinase, Tyrp1 contains a di-leucine-based sorting motif in its cytoplasmic domain that is necessary (although not sufficient – see ref. (17) for proper cellular localization (25) and binds in vitro to AP-1, which is enriched on endosomal buds in melanocytes (6). Tyrp1 is present at low levels at the plasma membrane and can be internalized, suggesting passage through endosomes during its life cycle (16,17,26,27), and a significant cohort of Tyrp1 can be found in transferrin-accessible endosomes at steady state in melanocytes (18)(C. Delevoye and G. Raposo, unpublished data). Tyrp1 distribution is altered by overexpression of a dominant negative form of the late endosomal GTPase, Rab7, in amelanotic cells or by Rab7 depletion in B16 mouse melanoma cells (28,29). Finally, Tyrp1 becomes trapped in early endosomes in melanocytes derived from HPS models lacking subunits of BLOC-1 or BLOC-2, suggesting that these complexes might function in transport between early endosomes and melanosomes (18). However, to date proof of such a pathway in melanocytic cells from non-mutant backgrounds is lacking.

In this study we sought to better define the role of early endosomes in the trafficking of Tyrp1 to melanosomes and to explore the mechanisms by which Tyrp1 trafficking is regulated. Our results show that newly synthesized Tyrp1 traverses early endosomes but not the cell surface en route to melanosomes, and provide evidence that ESCRT-I, but not the ESCRT-0 component Hrs, functions in this pathway at a step downstream of the HPS-associated BLOC-1.

Results

Internalization of cell surface Tyrp1 to early endosomes

At steady state, Tyrp1 localizes predominantly to melanosomes (5,18,25), but is expressed at low levels on the cell surface in a wide variety of melanoma and melanocyte cell lines (26,30) and can be internalized (16-18,27). The cell surface pool could thus potentially be targeted to melanosomes. To test whether the cell surface functions as an intermediate in the delivery of Tyrp1 to melanosomes, we investigated the fate of the cohort of cell surface Tyrp1 in melanocytic cells. The extent of cell surface Tyrp1, as determined by immunofluorescence microscopy (IFM) analysis of cells labeled on ice with the anti-Tyrp1 mAb TA99 prior to fixation, showed extensive variability among several pigmented cell lines (data not shown) and within a given cell population (e.g. see Fig. 1a). Easily detectable levels were observed in the immortalized mouse melanocyte cell line, melan-a, derived from wild-type C57BL/6J mice (31). Interestingly, the antibody did not label the cell surface uniformly, but instead showed a punctate staining pattern, suggesting that Tyrp1 at the plasma membrane of wild-type melanocytes may be enriched in specific subdomains such as clathrin-coated pits (as observed in BLOC-1-deficient melanocytes; ref. 18).

To determine whether cell surface Tyrp1 was endocytosed, cells with surface-bound TA99 antibody were warmed to 37° C for various times to allow for the antigen/ antibody complex to internalize. At each time point, remaining cell surface Tyrp1 was quantified by flow cytometry after incubating the cells on ice with a fluorescently tagged secondary antibody. As shown in Fig. 1b, Tyrp1 was rapidly internalized at a rate of 18.4% per min for the first 5 min, reminiscent of the kinetics of clathrin-dependent endocytosis. Similar results were obtained in other pigmented melanocytic cell lines (18).

We next sought to determine the fate of internalized Tyrp1 by IFM analysis of internalized anti-Tyrp1 antibody TA99 that was directly conjugated to Alexa^{594}. To ensure that the antibody did not dissociate from Tyrp1 during intracellular trafficking, we first tested whether TA99-Alexa^{594} remained bound to Tyrp1 under the acidic environment of endosomes and melanosomes. Fixed, permeabilized melan-a cells were incubated with TA99-Alexa^{594} at pH 7.4, washed, and then incubated for an additional 30 min in buffer of varying pH. Cells were then washed and fluorescence intensity was quantified by flow cytometry. Importantly, fluorescence intensity was identical when cells were incubated at pH 7.4 or pH 4.4 (Suppl. Fig. S1), demonstrating that TA99 remained bound to Tyrp1 at a pH below that expected for the endocytic and melanosomal pathways. Thus, the fate of internalized antibody should reasonably report on the fate of internalized Tyrp1. Moreover, since the Alexa^{594} moiety would not be expected to be degraded by lysosomal hydrolases, delivery of internalized Tyrp1 to late endosomes or lysosomes should be detectable by this approach.

To examine the cellular location of internalized Tyrp1 we plated melan-a cells on coverslips and incubated with TA99-Alexa^{594} on ice followed by incubation at 37°C for 5 min to allow the antibody/antigen complex to internalize. Internalization was then arrested at 0°C and cells were processed for IFM and colabeled for syntaxin 13, which localizes to early endocytic compartments including recycling endosomes (18,32). TA99-Alexa^{594} was observed on punctate structures that were also positive for syntaxin 13 (Fig. 1c-e, insets), confirming internalization to early endosomes. The few TA99-positive structures that did not colocalize with syntaxin 13 likely represent TA99 that had not been internalized within the 5 min incubation, consistent with the kinetic data.

Most internalized Tyrp1 remains localized to early endosomes by endocytic recycling and is only inefficiently delivered to melanosomes

We next tested whether the pool of cell surface Tyrp1 that was internalized into early endosomes eventually reached late melanosomes. Melan-a cells plated on coverslips were incubated with TA99-Alexa^{594} on ice followed by a 5 min uptake at 37°C to enhance labeling of the pool of cell surface and early endosomal Tyrp1. The cells were then washed and subsequently incubated at 37°C in growth medium without antibody for 20 or 60 min to allow for post-endocytic trafficking of the Tyrp1/antibody complex. The cells were then fixed and analyzed by IFM after costaining with markers of various organelles (Fig. 2).

In MNT-1 melanoma cells (5) and other cell types (33), 20 min of chase is sufficient time for endocytic cargoes to reach late endosomes. Late endosomes in melan-a cells were identified by labeling for lysobisphosphatidic acid (LBPA), a lipid that is present on internal membranes of late endosomal multivesicular bodies (34-36). After 20 min of chase in melan-a cells, internalized TA99-Alexa^{594} did not appreciably overlap by IFM with LBPA (Fig. 2a-c), indicating that little if any Tyrp1 accesses late endosomes within this time frame; since the free Alexa dye would not be expected to be degraded by lysosomal hydrolases, it is unlikely that the lack of overlap with LBPA reflects degradation of the antibody within these compartments. Moreover, the internalized TA99-Alexa^{594} did not overlap at all with Pmel17, indicating that internalized Tyrp1 does not reside appreciably within stage II melanosomes. By contrast, a small fraction of internalized TA99-Alexa^{594} in most cells colocalized with the steady state cohort of Tyrp1, labeled by post-fixation staining with TA99 conjugated to Alexa^{488} (Fig. 2g-i), as well as with pigment granules visualized by bright field microscopy (data not shown). Because most Tyrp1 at steady state is present in mature melanosomes (5), this suggests that a cohort of internalized Tyrp1 accessed mature stage III and IV melanosomes without significant accumulation in late endosomal or immature stage II melanosomes. Nevertheless, the majority of internalized TA99 in most cells did not colocalize with the steady state pool of Tyrp1 (Fig 2g-i), but

rather largely overlapped with labeling for syntaxin 13 (Fig. 2j-l). These observations suggest that internalized Tyrp1 is inefficiently transported to melanosomes within 20 min of chase, and that the majority remains associated with early endosomes. Importantly, nearly identical results were obtained when the chase was increased from 20 min to 60 min; the majority of internalized TA99 was still detected on syntaxin 13-positive structures (Fig. 3j-l) with a fraction reaching late stage melanosomes (Fig. 3g-i). Again, no significant labeling was detected in late endosomes (Fig. 3a-c) or stage II melanosomes (Fig. 3d-f). The poor delivery to melanosomes was not due to aberrant trafficking induced by antibody cross-linking because identical results were obtained using Alexa Fluor-conjugated TA99 F_{ab} fragments (Suppl. Fig. S1b-g). Moreover, similar results were obtained with human 1011-mel and MNT-1 melanoma cells, although the signal from internalized TA99 antibody was much weaker due to low plasma membrane labeling at time 0 (data not shown). Taken together, these data demonstrate that cell surface Tyrp1 is inefficiently trafficked to mature melanosomes, and that the minor cohort that does traffic to melanosomes does not pass significantly through late endosomes or stage II melanosomes.

The large fraction of cell surface-derived Tyrp1 found in syntaxin13-positive compartments after extended chase times suggested that Tyrp1 might undergo constitutive recycling. To test this, we used a quantitative fluorescence quenching assay to monitor the re-expression of internalized, fluorescently-labeled TA99 antibody at the cell surface (see Materials and Methods and (37). As shown in Fig. 4, recycled Tyrp1 was detectable by 5 min of chase and had reached 37% and 54% of the internalized pool, respectively, by 20 and 60 min of chase. Similar results were obtained with a second pigmented melanocyte cell line (18). These results were consistent with the IFM data and indicated that a majority of cell surface Tyrp1 underwent constitutive endocytic recycling.

Tyrp1 is sorted to melanosomes from within an intracellular compartment

The inefficient delivery of internalized Tyrp1 to melanosomes and the very high steady state distribution to melanosomes suggests that the cell surface pool of Tyrp1 does not contribute significantly to the predominant pool of Tyrp1 in melanosomes, and that the majority of newly synthesized Tyrp1 must thus be sorted to melanosomes independently of the cell surface. If this is the case, then the cell surface pool of Tyrp1 might not derive from the biosynthetic pathway. To test this prediction, we quantified the delivery of Tyrp1 to the cell surface over time using a continuous TA99-Alexa^{488} antibody uptake assay at 37°C in melan-a cells. As shown in Fig. 5a, uptake of anti-Tyrp1 antibody was biphasic, with more rapid uptake within the first 20 min, and then a more gradual uptake through 60 min. This biphasic curve likely represents a combination of two sources of Tyrp1: 1) a fast delivery representing recycling Tyrp1 delivered from early endosomes, which is consistent with the majority of recycling occurring by 20 min (Fig. 4), and 2) a sustained delivery from another intracellular source of Tyrp1. To determine whether the sustained delivery of Tyrp1 originated from the biosynthetic pathway, we treated the cells with Brefeldin A (BFA), which disrupts biosynthetic transport and redistributes Golgi membranes to the endoplasmic reticulum (38,39). Whereas treatment of cells with 10 μM BFA was sufficient to disperse the Golgi, based on the relocalization of GM130 to peripheral puncta (Fig. 5b, c), it had no effect on the kinetics of cell surface delivery of Tyrp1 (Fig. 5a). This indicated that the cell surface Tyrp1 does not originate from the biosynthetic pool but instead is supplied from another intracellular source. Interestingly, while BFA has been shown to inhibit recycling of TfR (40,41), Tyrp1 recycling was not affected by treatment with BFA (Fig. 4), consistent with the lack of effect on the rapid phase of cell surface delivery. Thus these data indicated that the cell surface pool of Tyrp1 derives predominantly from endocytic recycling, but not from the biosynthetic pool. Taken together, the data suggest that newly-synthesized Tyrp1 bypasses the plasma membrane en route to late melanosomes.

Hrs overexpression traps Tyrp1 in endosome-derived membrane clusters

The data presented above are consistent with either direct transport of Tyrp1 from the TGN to melanosomes or indirect transport via an endosomal compartment. To determine whether Tyrp1 traverses early endosomes en route to melanosomes in non-mutant melanocytes, we tested whether overexpression of Hrs affected Tyrp1 transport. Hrs is a component of the "ESCRT-0" complex involved in ILV formation within vacuolar endosomes (reviewed in (12-14)) and is enriched in the clathrin-containing coats of stage I melanosomes (15). Overexpression of Hrs in many cell types (42-47), including melanocytes (15), results in the formation of clusters of enlarged Hrs-positive endosomal structures that trap proteins associated with or passing through endocytic compartments. Hrs overexpression can therefore be used as a way to "trap" cargoes that normally traverse early endosomes, much in the same way that overexpression of dominant mutants of Rab5 has been used (48). We first overexpressed Hrs in the human melanoma cell line 1011-mel, which is easily transduced by transient transfection and faithfully segregates Tyrp1 to melanosomes. Twenty-four hrs after transient transfection with myc-tagged Hrs, 1011-mel cells were analyzed by IFM for the distribution of early endosomal markers and for Tyrp1 (Fig. 6). Overexpressed Hrs was concentrated in large structures that clustered near the perinuclear region of the cell and in smaller Hrs-positive structures in the cell periphery (Fig. 6a,d,g). We have previously shown that these structures trap cargoes destined for ILVs, including MART-1, epidermal growth factor receptor, and ubiquitylated proteins (15). As expected, other endosomal proteins, including EEA1, the transferrin receptor (TfR), and syntaxin 7 (a t-SNARE that regulates traffic between early and late endosomes (49,50)) were also significantly redistributed to the perinuclear Hrs-positive structures (Fig. 6b,e,h). These data confirm that Hrs overexpression acts as an early endosomal trap in 1011-mel cells.

Importantly, the majority of Tyrp1 was also redistributed to the Hrs-positive structures in myc-Hrs overexpressing cells (Fig. 7a-c). Tyrp1 redistribution was observed as early as 16 hrs post-transfection, and was nearly stoichiometric by 26-36 hrs. Trapping was specific, as Pmel17, a constituent of early stage melanosomes, was largely excluded from the Hrs-positive membranes at these time points (15). Golgi markers were also excluded from these structures (not shown). By immuno-electron microscopy (IEM), the Hrs-positive structures appeared as clusters of closely apposed vacuolar compartments, some of which contained internal membranes and all of which were densely decorated by antibodies to Hrs (Fig. 7d). The limiting membranes of some of these compartments were labeled by antibodies to Tyrp1 (arrows, Fig. 7d and inset), and labeling for Tyrp1 was not detected elsewhere (data not shown). Trapping of Tyrp1 in Hrs-positive membranes was also observed when Hrs was overexpressed in melan-a cells (Suppl. Fig. S2). Indeed, as shown in Fig. 5a, Hrs overexpression in melan-a cells significantly decreased levels of surface Tyrp1, slowed the rate of Tyrp1 delivery to the cell surface, and eliminated the rapid phase of Tyrp1 cell surface delivery during the first 20 minutes (which we interpret to reflect endocytic recycling), all consistent with an interference with endocytic cycling and melanosome delivery. These data suggest that Tyrp1 traffics though early endosomal compartments before reaching melanosomes.

Tyrp1 trafficking from endosomes to melanosomes does not require Hrs

Hrs is a docking protein that can simultaneously interact with multiple effectors (51,52). Thus, Hrs overexpression interferes with the concerted activity of any number of these effectors, such that the consequences of Hrs overexpression do not necessarily reflect interference with Hrs function *per se*. To determine whether Hrs is required for Tyrp1 sorting, we used siRNA to deplete Hrs from a different human melanoma cell line, MNT-1 (which is more amenable to siRNA effects than either melan-a or 1011-mel), and analyzed the effects on Tyrp1 distribution. As previously shown (15), Hrs depletion in MNT-1 cells

results in substantial down-regulation of MART-1, a melanocyte-specific protein that is targeted to lysosomes in a manner dependent on ubiquitylation (11) and on downstream ESCRT components (see below). By contrast, Tyrp1 distribution was grossly unaltered by Hrs depletion. By IEM, Hrs-depleted cells were significantly depleted of multivesicular structures as expected (53-56), accumulated vacuolar endosomes that were more abundant and enlarged compared to control cells (Suppl. Fig. S3a,c), and were depleted of MART-1 (not shown; see Ref. (15). However, Tyrp1 in these cells remained localized to mature melanosomes (Suppl. Fig. S3b). These data indicated that although Tyrp1 sorting from early endosomes is blocked by Hrs overexpression, it does not require Hrs function for delivery to the limiting membrane of melanosomes.

Tyrp1 trafficking to the melanosome limiting membrane requires ESCRT-I

One of the best-known effectors with which Hrs interacts to regulate endosomal protein sorting is ESCRT-I. Although Hrs and ESCRT-I cooperate to facilitate protein sorting to internal vesicles of MVBs (53,57-60), ESCRT-I and downstream ESCRT complexes participate in additional pathways, such as autophagy (61-63) and cytokinesis (64-66), and loss of ESCRT or Hrs function has differential effects on endosomal membrane dynamics (54,61). We therefore tested whether ESCRT-I is required for Tyrp1 sorting from late endocytic cargo.

We first used siRNA to deplete Tsg101 from MNT-1 melanoma cells. As shown in Fig. 8a, transduction of MNT-1 cells with Tsg101 siRNA resulted in a loss of >90% of detectable Tsg101 relative to cells transduced with control siRNA, concomitant with a marked loss of detectable Hrs. Surprisingly, although there was a reduction in overall melanin levels in cells treated with Tsg101 siRNA relative to controls (Suppl. Fig. S4a) and some cells had clearly reduced pigmentation relative to untreated cells (e.g. Fig. 8, compare panels **e** to **h**), many of the obviously Tsg101-depleted cells retained dense pigment granules in numbers comparable to those in control cells, suggesting that ESCRT-I is not absolutely required for pigmentation. Tsg101 depletion had no consistent effect on steady state levels of Tyrp1, but as expected, it interfered with MART-1 degradation resulting in a 2.5× increase in MART-1 levels relative to control cells (Fig. 8a). Consistently, whereas IFM analysis of control cells showed a faint, diffuse distribution of MART-1 concentrated near the pericentriolar region, MART-1 accumulated in enlarged, rounded structures throughout the cytoplasm in cells depleted of Tsg101 (Fig. 8b,c).

Importantly, Tyrp1 in Tsg101-depleted cells also accumulated in large rounded structures (Fig. 8d,g) that only partially overlapped with those harboring MART-1 (Fig. 8j-o), consistent with the distinct destination of these two cargoes. Compared to the characteristic ring-like strucutres surrounding pigment granules in control cells, the Tyrp1-containing structures in Tsg101-depleted cells tended to be enlarged, less uniform, and did not surround the pigment granules (Fig. 8d-i). This suggested that Tyrp1 was no longer present on the limiting membrane of melanosomes. Indeed, IEM analyses revealed that whereas in control cells Tyrp1 was predominantly localized to melanosomes (Fig. 9a), Tyrp1 in Tsg101 siRNA-treated cells was depleted from melanosomes and accumulated on unusually abundant, often electron dense membranous structures with irregular internal membranes, not unlike autophagosomes, and in vacuole-like membrane delimited structures with a clear lumen close to melanosomes (Fig. 9c, e). MART-1, which in control cells was detected on multivesicular endosomes (Fig. 9b), the Golgi and endosomes as described (8), was instead detected on electron dense membranous structures in Tsg101-depleted cells, like Tyrp1, but also in extensive tubulated membranes similar to those described in Tsg101-depleted A431 and HEK293 cells (54)(Fig. 9d). Consistent with the IFM analysis, labeling for Tyrp1 and MART-1 only partially overlapped and each was largely distributed on distinct membranes (Fig. 9e). Both MART-1- and Tyrp1-containing membranes were distinguishable from

separate multivesicular compartments that persisted in Tsg101-depleted cells and that harbored the bulk of Pmel17 on intralumenal membranes (Suppl. Fig. S3d,e). As in wild-type cells (Fig. 10Ag-i), most of the Tyrp1-containing structures in these cells were not labeled for EEA1, suggesting that they do not correspond to early endosomes (Fig. 10Aj-l). By contrast, a subset of them – particularly the enlarged, rounded structures - were labeled by antibodies to the late endosomal/ lysosomal membrane protein LAMP1 (Fig. 10Aa-f). IEM analyses indicated that the LAMP1- and Tyrp1-containing structures corresponded primarily to the vacuole-like membranes near melanosomes (Fig. 10B). Together, these data suggest that the ESCRT-I component Tsg101 is required for the selective delivery of Tyrp1 to melanosomes and for the segregation of Tyrp1 from lysosomal cargoes within transport intermediates.

To corroborate a role for ESCRT-I in Tyrp1 trafficking using different methodology, we assayed Tyrp1 steady state localization in cells overexpressing dominant inhibitors of the ESCRT pathway. 1011-mel cells were transfected with an ATP-binding deficient mutant of hVps4B (hVps4B.K173A; referred to here as dnVps4), which has been used previously to inhibit Vps4 activity in recycling ESCRT-III components from membranes (67) and which effectively blocks sorting of ubiquitylated cargoes, such as MART-1 and EGF receptor, to lysosomes in 1011-mel cells (15). IFM analyses showed that like in Tsg101-depleted cells, Tyrp1 in cells overexpressing dnVps4 accumulated in large aberrant rounded structures (Fig. 11a-c) that overlapped extensively with labeling for LAMP1 (Fig. 11d-f, **arrows**). By contrast, very little overlap between Tyrp1 and LAMP1 was detected in untransfected cells. This suggested that like depletion of the ESCRT-I component Tsg101, gross inhibition of the ESCRT pathway blocks the segregation of Tyrp1 from late endosomal/ lysosomal components. To extend these data, we assayed Tyrp1 localization in cells overexpressing Tsg101. Like dnVps4, overexpression of Tsg101 in 1011-mel cells blocks trafficking of ubiquitylated cargoes like MART-1 (15). Tyrp1 was difficult to detect in most Tsg101-overexpressing cells by IFM (compare the starred cell in Fig. 11g-i to the untransfected cell on the right) or by IEM (data not shown), in which Tsg101 accumulated in cytoplasmic inclusions that appear as rings by IFM (Fig. 11g). Immunoblotting also showed a reduction in Tyrp1 levels (data not shown). Tyrp1 in these cells was likely degraded by lysosomal proteases within aberrant endosome-derived structures that result from Tsg101 overexpression, since treatment of the cells for 4 hrs with the vacuolar ATPase inhibitor, bafilomycin A1, restored Tyrp1 expression as detected by IFM (data not shown). In rare cases, Tyrp1 in cells that mildly expressed Tsg101 (Fig. 11g-i, **arrows**) was detected at high levels within large vacuolar structures, much like in cells overexpressing dnVps4 or depleted of Tsg101. We interpret these effects as an interference with the segregation of melanosomal and lysosomal cargoes, with consequent degradation of Tyrp1 by lysosomal proteases in cells with high Tsg101 expression.

Analyses of Tyrp1 trafficking in HPS model melanocytes suggests that BLOC-1 is required to sort Tyrp1 out of early endosomal domains toward melanosomes (18). In the absence of BLOC-1, Tyrp1 undergoes constitutive cycling between early endosomes and the plasma membrane, resulting in a large increase in the flux of Tyrp1 through the plasma membrane (18). To determine whether ESCRT-I functions upstream or downstream of BLOC-1, we tested whether Tsg101 depletion altered the flux of Tyrp1 through the plasma membrane. Cells treated with control or Tsg101 siRNA were incubated with anti-Tyrp1 antibody at 37°C for 10-60 min, and the internalized antibody was quantified using a quantitative fluorescence microscopy assay. In MNT-1 cells treated with either control or Tsg101 siRNAs, uptake was unmeasurable at 10 min and increased as expected from 30 to 60 min (not shown). However, Tsg101 depletion dramatically reduced the flux of Tyrp1 through the plasma membrane relative to control cells after 30 (not shown) and 60 min of uptake (Fig. 10C). These data suggest that depletion of Tsg101 blocks Tyrp1 trafficking at a step

downstream of the decision to recycle to the plasma membrane, and thus downstream of BLOC-1, and are consistent with the partial localization of Tyrp1 with LAMP1 in these cells (Fig. 10A, B).

Taken together, these data indicate that minimally ESCRT-I, and perhaps additional downstream ESCRT components, are required to ensure Tyrp1 steady state localization to the mature melanosome limiting membrane. Moreover, they suggest that ESCRT-I functions from an endosomal domain downstream of classical early endosomes, and further confirm that specific endosomal domains are obligate intermediates in the biosynthetic transport of Tyrp1 to melanosomes.

Discussion

In this study we have characterized the intracellular trafficking pathway by which Tyrp1 accesses melanosomes in pigmented eumelanogenic melanocytes. Our results show that newly-synthesized Tyrp1 is transported from the Golgi to mature melanosomes via an endosomal intermediate, within which it is sorted away from both late endocytic and pre-melanosomal cargoes. At a later stage, likely following delivery to mature melanosomes, a small fraction of Tyrp1 is targeted to the cell surface, from where Tyrp1 is internalized into early endosomes. In contrast to the biosynthetic pool of Tyrp1, however, this pool of Tyrp1 is inefficiently transported to mature melanosomes and undergoes endocytic recycling. Thus, Tyrp1 exists within melanocytes in two pools, both of which pass through endocytic compartments but with different kinetics and distinct destinations. Finally, we show that proper accumulation of Tyrp1 in melanosomes requires ESCRT-I and is blocked by dominant inhibitors of generalized ESCRT function, suggesting that ESCRT-I and perhaps downstream ESCRT components function in the pathway from endosomes to melanosomes. These findings confirm a role for early endosomes in the intracellular transport of a melanosome-specific protein and have important implications for understanding the relationship between endosomal trafficking and the biosynthetic sorting of proteins, the mechanisms controlling these trafficking pathways, and the role of ESCRT components in endosomal trafficking processes other than MVB formation.

Previous studies have shown that other melanosomal proteins, particularly Pmel17 (5,15,68-72) and tyrosinase (6,7), traverse distinct domains of early endosomes in pigment cells en route to melanosomes. We show here that disruption of early endosomal trafficking by Hrs overexpression depletes Tyrp1 from mature melanosomes, indicating that Tyrp1 also traverses early endosomes en route to melanosomes. Our conclusions are consistent with 1) the altered distribution of Tyrp1 upon disruption of the endosomal GTPase, Rab7 (28,29) or of Rab32 and Rab38 (73), 2) the accumulation of Tyrp1 in endosomes of BLOC-1- and BLOC-2-deficient melanocytes from mouse HPS models (18), and 3) the misaccumulation of Tyrp1 and tyrosinase in endosomes of glycosylceramide-deficient melanocytes (17). Our data using wild-type melanocytes support the notion that the misaccumulation of Tyrp1 in endosomes in mutant melanocytes represents a block in a bona fide trafficking intermediate. Because Tyrp1 is long-lived (half-life > 8 hrs in our cells) and prolonged Hrs overexpression causes indirect phenotypes in our cells (see ref. (15), we could not distinguish whether the mislocalized Tyrp1 in Hrs-overexpressing cells derived exclusively from newly synthesized material or partially from a cohort that was recycled from melanosomes. Ongoing anlyses of Tyrp1 dynamics in living cells might distinguish these possibilities.

While passage through early endocytic compartments is required for proper cellular localization, we show that sorting from the plasma membrane is dispensable. Internalized Tyrp1 reached mature melanosomes only inefficiently, and blocking biosynthetic export had no effect on cell surface delivery of Tyrp1. While it is possible that antibody binding to

Tyrp1 might interfere with a lumenal glycosphingolipid-dependent sorting determinant (17), we feel that this is unlikely given that such a mechanism would be expected to interfere completely with antibody delivery to melanosomes, and yet we observed a significant cohort of internalized anti-Tyrp1 antibody within melanosomes by 20 min of uptake. The cohort of cell surface Tyrp1 does not appear to derive from the newly synthesized pool as evidenced by the inability of brefeldin A to block routing of Tyrp1 through the plasma membrane. Our data are consistent with previous reports (16-18), and provide strong evidence that newly synthesized Tyrp1 does not significantly cycle through the plasma membrane en route to melanosomes. This contrasts with Pmel17, which appears to largely traverse the plasma membrane en route to stage II premelanosomes since a natural mutation in *silver* mice that eliminates the endocytic signal significantly depletes Pmel17 from premelanosomes (68).

Why is cell surface-derived Tyrp1 inefficiently targeted to melanosomes? One potential explanation is that biosynthetic and endocytic pools of Tyrp1 access distinct early endosomal domains with differential abilities to divert cargo to melanosomes. Targeting of Tyrp1 to these distinct pools would then reflect differential entry into membrane microdomains at the source membrane, i.e. the plasma membrane or the TGN (17,27). A second potential explanation is that only the biosynthetic pool associates with a “chaperone” that associates with and ferries Tyrp1 to melanosomes, and that this chaperone would be lost during subsequent cell surface routing. This possibility would be consistent with the requirement for the Tyrp1 lumenal domain in sorting to melanosomes (17).

The cohort of Tyrp1 that accesses the plasma membrane in wild-type melanocytes is insensitive to brefeldin A but sensitive to Hrs overexpression and Tsg101 depletion, and thus likely derives from a post-endosomal pool. The most likely source membrane is the melanosome itself. The cohort of cell surface Tyrp1 could thus reflect transient fusion of melanosomes with the plasma membrane, as suggested by some models of melanin transfer (74), or vesicular or tubular transport from melanosomes to the plasma membrane. Alternatively, it is possible that a small cohort of Tyrp1 remains largely trapped in endosomes even in wild-type cells, with occasional release toward the plasma membrane.

The precise nature of the endosomal intermediates through which Tyrp1 passes en route to melanosomes is not yet clear. A redistribution of Tyrp1 observed upon overexpression of a dominant negative Rab7 or depletion of Rab7 by antisense oligonucleotide expression (28,29) has been interpreted as reflecting a sorting pathway from late endosomes to melanosomes. However, Rab7 is known to function in other cell types in early to late endosome traffic (75-77) and its activity might thus be required to release Tyrp1-containing vesicles from early endosomes or from the transport vesicles derived therefrom. Rab7 also plays a major role in melanosome motility (78), perhaps explaining the effect of altered Rab7 function on Tyrp1 distribution. Neither steady state Tyrp1 nor internalized Tyrp1 is detected in LAMP1- or LBPA-containing late endosomes, suggesting that sorting of Tyrp1 might occur through a subdomain of early endosomes. This is supported by the requirement for BLOC-1 in Tyrp1 delivery (18) given that BLOC-1 localizes to early endosomal tubules (16), and by the requirement for endosomal AP-1 in Tyrp1 transport (C. Delevoye and GR, unpublished results). The entrapment of Tyrp1 in Hrs-coated structures upon Hrs overexpression shown here also supports this model.

The results of this study emphasize the importance of the early endosome as a critical intermediate in the transport of components of lysosome-related organelles such as melanosomes. Whereas Tyrp1, tyrosinase and Pmel17 are all transported to melanosomes via early endosomes, all three cargoes appear to do so via different pathways and likely from distinct endosomal domains. The plasticity of early endosomes to facilitate multiple sorting pathways likely underlies the variable phenotypes of diseases of lysosome-related organelle

biogenesis, such as HPS (79-81). Our data here and elsewhere (18) suggest that BLOC-1 and BLOC-2, defective in several variants of HPS, interfere with a physiological pathway from early endosomes to melanosomes.

It is intriguing that Tyrp1 trafficking was blocked in cells in which ESCRT-I is depleted or in which ESCRT function is generally inhibited by dominant-negative overexpression of inactive Vps4 or of Tsg101. The redistribution of Tyrp1 observed upon these treatements was specific, since Pmel17 invagination onto ILVs was not affected. The precise mechanism by which ESCRT proteins regulate endosomal membrane dynamics is still unclear, but their best characterized role is in formation of ILVs and sorting ubiquitylated cargo to them (9). It is thus surprising that interference with ESCRT-I function affects the localization of a component that ultimately resides on the limiting membrane of melanosomes rather than on internal membranes. One potential explanation for the effect is that ESCRTs facilitate removal of ILV cargoes from the limiting membrane of the forming transport intermediate, and thereby segregate lysosomal cargo from Tyrp1 and other melanosome-bound components; thus only limiting membrane components would be free to traffic to melanosomes. When ESCRT function is disrupted, ILV cargo would fail to segregate from Tyrp1. Alternatively, Tyrp1 might indeed segregate with ILVs, but ESCRT-I might then be required to “rescue” Tyrp1 from the ILVs through “back-fusion” as proposed for cytoplasmic release of viral RNA from endosomal vesicular stomatitis virus (82). Thirdly, disruption of ESCRT function might have global effects on endosomal membrane dynamics, as observed in other systems (54), with indirect effects on Tyrp1 sorting. Such global effects might lead to formation of arrested autophagy intermediates containing expanded endosomal membranes (61,62), perhaps explaining why Tyrp1 and the ubiquitylated cargo protein, MART-1, were observed in autophagosome-like structures of Tsg101-depleted cells. Indeed, a recent report has implicated autophagy regulatory proteins in melanosome biogenesis (83). A fourth non-mutually exclusive possibility is that ESCRT-I participates in formation of an endosomal sub-domain from which Tyrp1 can be delivered to melanosomes. Such domains might be similar to electron dense coats of Hep2 cell vacuolar endosomes that lack Hrs and clathrin (84) and that are stabilized by dominant negative Vps4 expression (85). Finally, ESCRT-I might function by coupling endosomal domains to additional machinery involved in Tyrp1 delivery to melanosomes, such as BLOC-1 (18) or AP-1 (5,6); indeed, evidence for an interaction of AP-1 and Tsg101 has recently been published (86). On the other hand, the reduction in Tyrp1 flux through the plasma membrane and colocalization of Tyrp1 with LAMP1 in Tsg101-depleted cells contrasts with the dramatic increase in Tyrp1 flux through the plasma membrane and colocalization with early endosomal markers in BLOC-1-deficient cells, and suggests that Tsg101 acts downstream of BLOC-1 in the Tyrp1 cargo delivery pathway. Interestingly, while ESCRT-I depletion inhibited Tyrp1 segregation from lysosomal cargo, depletion of Hrs had no effect on Tyrp1 delivery to mature melanosomes. This raises the possibility that Tyrp1 sorting is only affected by distinct components of the ESCRT pathway, consistent with the differential steady state distribution of Tsg101 and Hrs in HeLa cells (53) and the differential roles for Hrs and Tsg101 in MVB formation and EGF down-regulation (54), autophagy (61), and viral RNA release (82).

Our results thus emphasize the multiplicity of membrane trafficking pathways controlled by ESCRTs. While originally thought to regulate primarily inward budding in MVBs and topologically related viral budding from the plasma membrane (87), it is now clear that ESCRT components regulate a wide range of membrane dynamics including autophagy (62,88) and cytokinesis (64-66). Our study adds to this growing list of ESCRT-I functions the endosomal delivery of cargo to the limiting membrane of a lysosome-related organelle. The next challenge will be to determine how ESCRT-I contributes to this process and whether other ESCRT components function at the same step.

Materials and Methods

Cell culture and transfection

Human MNT-1, 1011-mel cells (5), and mouse melan-a cells (31) were cultured as described. Cells were transfected with plasmids using fuGENE-6 according to manufacturers' instructions using 2 μg of DNA (Roche Applied Science, Indianapolis, IN) and analyzed 24-48 hours post transfection. Where indicated, cells were treated with 10 μm BFA (Sigma, St. Louis, MO) or 100 nM bafilomycin A1 (EMD/ Calbiochem, San Diego, CA).

Chemicals and Reagents

All reagents used were obtained from Sigma unless otherwise noted.

Antibodies and fluorescent probes

Monoclonal antibodies, their targets and sources were as follows: anti-EEA1 and anti-GM130 were from BD Biosciences (San Jose, CA); B3/25 to human transferrin receptor was from Roche (Indianapolis, IN); TA99 to Tyrp1, 7G7.B6 to Tac and 9E10 to the myc epitope were from American Type Culture Collection (Manassas, VA); HMB45 to Pmel17 was from Lab Vision (Fremont, CA); 1D4B to human LAMP1 and H4A3 to mouse LAMP1 were from Developmental Studies Hybridoma Bank (Iowa City, IA); 4A10 to Tsg101 was from GeneTex (San Antonio, TX); and 6C4 to LBPA (34) was a kind gift from Jean Gruenberg (University of Geneva, Switzerland). Polyclonal antibodies, their targets and sources were as follows: Goat anti-V5 epitope was from Bethyl Laboratories (Montgomery, TX); Rabbit anti-V5 was from ICL (Newburgh, OR); A-14 to the myc epitope was from Santa Cruz Biotech (Santa Cruz, CA); rabbit antibodies to syntaxin 7 and syntaxin 13 were kind gifts from Andrew Peden (University of Cambridge, UK); and rabbit antibody to Hrs was a kind gift of Sylvie Urbé (University of Liverpool, UK). TA99-Alexa^{488} -Alexa^{594} and –PE were prepared using protein conjugation kits from Molecular Probes (Eugene, OR) and Prozyme (San Leandro, CA). TA99-Alexa^{594} F_{ab} was prepared by using an Immuno F_{ab} kit from Pierce (Rockford, Il). Fluorophore-conjugated species- and isotype-specific secondary antibodies were from Molecular Probes.

Plasmids

Myc epitope-tagged Hrs was from H. Stenmark (Dept. Biochemistry, The Norwegian Radium Hospital, Oslo, Norway) (89). hVps4b (K173A) with a C-terminal V5 epitope tag and human Tsg101 with an N-terminal HA epitope tag were from A. Pfeifer and P. Bates (University of Pennsylvania, Philadelphia, PA).

siRNAs

siRNA to human Hrs (15) and Tsg101 (90) have been described. The control siRNA in most experiments had the following sequence: 5′-AAUUCUCCGAACGUGUCACGdTdT -3′; for antibody uptake assays, a different control siRNA was used with the following sequence: 5′-AGAACAGUUGAUUCAGCGGdTdT-3′. All siRNAs were purchased from Qiagen, Inc. (Valencia, CA). MNT-1 cells were seeded at 10^5 per 10-cm dish, and then transduced the next day with 40 pmol siRNA using Oligofectamine (Dharmacon) in serum-free OptiMEM medium (InVitroGen) according to manufacturer's instructions. Two days later, cells were trypsinized, replated onto dishes with or without coverslips, and the next day the transfection was repeated. Cells were analyzed two to three days after the second transfection. For immunofluorescence microscopy, volumes, siRNA and cell numbers were reduced by 10-fold and Matrigel (BD Biosciences)-coated 12 well dishes were used for both primary and secondary transfections.

Immunoelectron Microscopy

Cells were fixed with 2% paraformaldehyde with or without 0.2% glutaraldehyde, and single- or double-immunogold labeling of ultrathin cryosections was performed as described (91) using protein A conjugated to 10 nm or 15 nm gold particles (PAG10 or PAG15) (purchased from the Cell Microscopy Center, Utrecht Medical School, Utrecht, the Netherlands).

Immunofluorescence Microscopy

Cells were fixed in 2-4% formaldehyde in PBS and stained as described (92) with indicated primary antibodies and secondary antibodies conjugated to Alexa^{488} and Alexa^{594} (Molecular Probes) and for triple labeling to AMCA (Jackson Immuno Research, West Grove, PA). In most experiments, cells were analyzed on a Leica Microsytems (Bannockburn, IL) DM IRBE microscope with a 63×, 1.4NA Plan Apo objective lens, and images were captured and processed using a Hamamatsu (Hamamatsu, Japan) Orca digital camera and Improvision (Lexington, MA) OpenLab software. Images shown are processed from sequential z-series images captured at 0.2 μm intervals and deconvolved using OpenLab Volume Deconvolution and represent 3 to 5 merged deconvolved planes. In some cases, MNT-1 cells were analyzed on a Leica Microsystemes (Nanterre, France) DM-RXA2 3D deconvolution microscope equipped with a piezo z-drive (Physik Instrumente, Pantin, France) and a 100×, 1.4NA-PL-APO objective lens for optical sectioning. Images shown are maximum-intensity z projections of 3D image stacks acquired using Metamorph software (MDS Analytical Technologies, Sunnyvale, CA) through a Coolsnap HQ (Photometrics, Tucson, AZ) cooled CCD-camera.

Qualitative antibody uptake

Melan-a cells plated on sterile glass coverslips were incubated in growth medium containing 25 mM HEPES and 400 nM TA99-Alexa^{594} for at least 30 min to allow binding to cell surface Tyrp1. The cells were placed at 37°C for 5 min to allow for antibody uptake and then plunged on ice. To determine the post endocytic fate of the antibody/antigen complex, the cells were washed twice with growth medium and then fixed either immediately in 2% formaldehyde for 20 min or incubated in growth medium for 20 min or 60 min before fixation. The cells were then processed for indirect immunofluorescence microscopy as described.

Quantitative cell surface delivery assay

1011-mel or melan-a cells were incubated in growth medium containing 100 nM TA99-Alexa^{488} for the specified times and then plunged on ice, washed twice with cold medium, and resuspended in FACS buffer (phosphate buffered saline + 5% FBS + 2mM EDTA + 0.2% Sodium Azide). Fluorescence was quantified by flow cytometry on a FACScan and analyzed using Cell Quest software (BD Biosciences). For BFA treatment, cells were treated with 10 μM BFA for 60 min prior to the experiment and BFA was included in the medium during subsequent incubations.

For MNT-1 cells transduced with control or Tsg101 siRNAs, cells grown on coverlips were incubated in growth medium supplemented with 50 μg/ ml TA99 antibody for 10, 30 or 60 min at 37°C. Cells were rinsed rapidly in warm PBS and then fixed on ice with 2% formaldehyde for 20 min. Cells were permeabilized, immunolabeled for MART-1 and for internalized TA99 antibody using isotype-specific Alexafluor-conjugated secondary antibodies, and analyzed by IFM. Effectiveness of Tsg101 knockdown was determined qualitatively by the increased intensity and altered pattern of MART-1 labeling. Images of TA99 labeling in these cells or controls were captured at identical exposure and gain

settings. The amount of internalized TA99 antibody in at least 50 cells of each type per experiment in two experiments was quantified using Improvision OpenLab software, and negative control values from each image were calculated from an area devoid of cells. The mean pixel intensity per cell was calculated by subtracting the negative control value, and then the average and variance values of these mean pixel intensity values were calculated for each data set. These values from two experiments were used to calculate a weighted average and standard deviation from a pooled variance for each condition.

Endocytosis assay

Melan-a cells were harvested with Trypsin-LE (Invitrogen, Carlsbad, CA), resuspended in growth medium containing 25 mM HEPES pH 7.4 and pelleted at 1200g for 2 min. One confluent T-75 flask (Corning Costar, Corning, NY) was used per 12-15 samples. The cells were resuspended in HEPES-buffered growth medium and 100 μl of cell suspension per sample was incubated with primary antibody on ice for at least 30 min to allow binding to the cell surface. The cells were transferred to 37°C for the indicated times to allow for endocytosis and then plunged in ice, pelleted, resuspended in FACS buffer containing Alexa^{488}-conjugated secondary antibody and incubated on ice for at least 30 min. The cells were washed twice in cold FACS buffer and the amount of cell surface fluorescence remaining after each time point was quantified by flow cytometry as described above.

Recycling Assay

Melan-a cells were harvested as described above. The cells were resuspended in HEPES-buffered growth medium and 100 μl of cell suspension per sample was incubated with 100 nM Alexa^{488}-conjugated TA99 antibody (or 7G7.B6-Alexa^{488} as a control) on ice for at least 30 min. The cells were washed twice with cold medium, incubated at 37°C for 5 min to internalize the antibody/antigen complex and then plunged on ice. Excess unlabeled TA99 and anti Alexa^{488} quenching antibody (or control anti-myc) were added and the cells were placed at 37°C for various times to allow for the internalized antibody/antigen complex to recycle back to the cell surface. Following the incubation the cells were placed on ice and incubated for a minimum of 20 min to ensure complete antibody/antigen binding. The cells were then washed twice with cold medium, resuspended in FACS buffer and remaining fluorescence was quantified by flow cytometry as described above. For BFA treatment, cells were treated with 10 μM BFA for 60 min prior to the experiment and BFA was included in the medium during subsequent incubations.

Antibody binding assay

Melan-a cells were harvested as described above. The cells were resuspended in FACS buffer, fixed in 2% formaldehyde/PBS for 15 min at RT, washed twice with PBS, and permeabilized in FACS buffer containing 0.2% saponin. The cell suspension was washed once with PBS and incubated with 100 nM Alexa^{488}-conjugated TA99 antibody (or Alexa^{488}-7G7.B6 as a control) on ice, with periodic mixing, for at least 60 min. The cells were washed twice with PBS and resuspended in 40 mM sodium phosphate, pH 7.4 or citrate-phosphate buffer (30 mM $C_6H_8O_7$, 45 mM Na_2HPO_4, pH 4.4) and incubated on ice, with mixing, for 30 min. The cells were washed 3 times with PBS, resuspended in FACS buffer and analyzed by flow cytometry as described above.

Melanin content assay

Melanin content in equal numbers of control and Tsg101 siRNA-treated cells was quanitifed essentially as described (73). Briefly, cells were disrupted by sonication in 50 mM Tris-HCl, pH 7.4, 2 mM EDTA, 150 mM NaCl and protease inhibitors. Pigment was pelleted at 20,000 g for 15 min at 4°C, rinsed once in ethanol/ether (1:1), and dissolved in 2 M NaOH/

20% dimethylsulfoxide at 60°C. Melanin content was measured as optical density at 492 nm.

Supplementary Material

Refer to Web version on PubMed Central for supplementary material.

Acknowledgments

We thank Jennifer-Marie Millado for technical assistance, Anand Sitaram for assistance with statistical analyses, Vincent Fraisier and Lucy Sengmanivong (PICT-IBiSA Imaging Facility, Institut Curie) for assistance with deconvolution microscopy, and Andrew Peden, Jean Gruenberg, Harald Stenmark, Sylvie Urbé, Paul Bates and Andrew Peifer for generous gifts of reagents. This work was supported by grant R01 EY015625 from the National Eye Institute/National Institutes of Health, by Institute Curie, Centre National de la Recherche Scientifique and Fondation pour la Recherche Médicale (GR), training grant T32-CA-009140 from the National Cancer Institute (STT and ACT), and a fellowship 062543U from the American Heart Association (SRGS)

References

1. Dell'Angelica EC, Mullins C, Caplan S, Bonifacino JS. Lysosome-related organelles. FASEB J. 2000; 14:1265–1278. [PubMed: 10877819]
2. Raposo G, Marks MS, Cutler DF. Lysosome-related organelles: driving post-golgi compartments into specialisation. Curr Opin Cell Biol. 2007; 19:394–401. [PubMed: 17628466]
3. Raposo G, Marks MS. Melanosomes - dark organelles enlighten endosomal membrane transport. Nat Rev Mol Cell Biol. 2007; 8:786–798. [PubMed: 17878918]
4. Seiji M, Fitzpatrick TM, Simpson RT, Birbeck MSC. Chemical composition and terminology of specialized organelles (melanosomes and melanin granules) in mammalian melanocytes. Nature. 1963; 197:1082–1084. [PubMed: 13992623]
5. Raposo G, Tenza D, Murphy DM, Berson JF, Marks MS. Distinct protein sorting and localization to premelanosomes, melanosomes, and lysosomes in pigmented melanocytic cells. J Cell Biol. 2001; 152:809–823. [PubMed: 11266471]
6. Theos AC, Tenza D, Martina JA, Hurbain I, Peden AA, Sviderskaya EV, Stewart A, Robinson MS, Bennett DC, Cutler DF, Bonifacino JS, Marks MS, Raposo G. Functions of AP-3 and AP-1 in tyrosinase sorting from endosomes to melanosomes. Mol Biol Cell. 2005; 16:5356–5372. [PubMed: 16162817]
7. Huizing M, Sarangarajan R, Strovel E, Zho Y, Gahl WA, Boissy RE. AP-3 mediates tyrosinase but not TRP-1 trafficking in human melanocytes. Mol Biol Cell. 2001; 12:2075–2085. [PubMed: 11452004]
8. de Mazière AM, Muehlethaler K, van Donselaar E, Salvi S, Davoust J, Cerottini JC, Lévy F, Slot JW, Rimoldi D. The melanocytic protein melan-A/MART-1 has a subcellular localization distinct from typical melanosomal proteins. Traffic. 2002; 3:678–693. [PubMed: 12191019]
9. Slagsvold T, Pattni K, Malerod L, Stenmark H. Endosomal and non-endosomal functions of ESCRT proteins. Trends Cell Biol. 2006; 16:317–326. [PubMed: 16716591]
10. Hurbain I, Geerts WJC, Boudier T, Marco S, Verkleij A, Marks MS, Raposo G. Electron tomography of early melanosomes: implications for melanogenesis and the generation of fibrillar amyloid sheets. Proc Natl Acad Sci USA. 2008; 105:19726–19731. [PubMed: 19033461]
11. Lévy F, Muehlethaler K, Salvi S, Peitrequin AL, Lindholm CK, Cerottini JC, Rimoldi D. Ubiquitylation of a melanosomal protein by HECT-E3 ligases serves as sorting signal for lysosomal degradation. Mol Biol Cell. 2005; 16:1777–1787. [PubMed: 15703212]
12. Babst M. A protein's final ESCRT. Traffic. 2005; 6:2–9. [PubMed: 15569240]
13. Raiborg C, Stenmark H. The ESCRT machinery in endosomal sorting of ubiquitylated membrane proteins. Nature. 2009; 458:445–452. [PubMed: 19325624]
14. Hurley JH, Emr SD. The ESCRT complexes: structure and mechanism of a membrane-trafficking network. Annu Rev Biophys Biomol Struct. 2006; 35:277–298. [PubMed: 16689637]

15. Theos AC, Truschel ST, Tenza D, Hurbain I, Harper DC, Berson JF, Thomas PC, Raposo G, Marks MS. A lumenal domain-dependent pathway for sorting to intralumenal vesicles of multivesicular endosomes involved in organelle morphogenesis. Dev Cell. 2006; 10:343–354. [PubMed: 16516837]

16. Di Pietro SM, Falcon-Perez JM, Tenza D, Setty SRG, Marks MS, Raposo G, Dell'Angelica EC. BLOC-1 interacts with BLOC-2 and the AP-3 complex to facilitate protein trafficking on endosomes. Mol Biol Cell. 2006; 17:4027–4038. [PubMed: 16837549]

17. Groux-Degroote S, van Dijk SM, Wolthoorn J, Neumann S, Theos AC, De Mazière AM, Klumperman J, van Meer G, Sprong H. Glycolipid-dependent sorting of melanosomal from lysosomal membrane proteins by lumenal determinants. Traffic. 2008; 9:951–963. [PubMed: 18373728]

18. Setty SRG, Tenza D, Truschel ST, Chou E, Sviderskaya EV, Theos AC, Lamoreux ML, Di Pietro SM, Starcevic M, Bennett DC, Dell'Angelica EC, Raposo G, Marks MS. BLOC-1 is required for cargo-specific sorting from vacuolar early endosomes toward lysosome-related organelles. Mol Biol Cell. 2007; 18:768–780. [PubMed: 17182842]

19. Jackson IJ. A cDNA encoding tyrosinase-related protein maps to the brown locus in mouse. Proc Natl Acad Sci USA. 1988; 85:4392–4396. [PubMed: 3132713]

20. Halaban R, Moellmann G. Murine and human b locus pigmentation genes encode a glycoprotein (gp75) with catalase activity. Proc Natl Acad Sci USA. 1990; 87:4809–4813. [PubMed: 1693779]

21. Kobayashi T, Imokawa G, Bennett DC, Hearing VJ. Tyrosinase stabilization by Tyrp1 (the *brown* locus protein). J Biol Chem. 1998; 273:31801–31805. [PubMed: 9822646]

22. Vijayasaradhi S, Bouchard B, Houghton AN. The melanoma antigen gp75 is the human homologue of the mouse b (brown) locus gene product. J Exp Med. 1990; 171:1375–1380. [PubMed: 2324688]

23. Liu TF, Kandala G, Setaluri V. PDZ-domain protein GIPC interacts with the cytoplasmic tail of melanosomal membrane protein gp75 (tyrosinase related protein-1). J Biol Chem. 2001; 276:35768–35777. [PubMed: 11441007]

24. Chapuy B, Tikkanen R, Mülhausen C, Wenzel D, von Figura K, Höning S. AP-1 and AP-3 mediate sorting of melanosomal and lysosomal membrane proteins into distinct post-Golgi trafficking pathways. Traffic. 2008; 9:1157–1172. [PubMed: 18410487]

25. Vijayasaradhi S, Xu YQ, Bouchard B, Houghton AN. Intracellular sorting and targeting of melanosomal membrane proteins: identification of signals for sorting of the human brown locus protein, gp75. J Cell Biol. 1995; 130:807–820. [PubMed: 7642699]

26. Xu Y, Setaluri V, Takechi Y, Houghton AN. Sorting and secretion of a melanosome membrane protein, gp75/TRP1. J Invest Dermatol. 1997; 109:788–795. [PubMed: 9406822]

27. Sprong H, Degroote S, Claessens T, van Drunen J, Oorschot V, Westerink BHC, Hirabayashi Y, Klumperman J, van der Sluijs P, van Meer G. Glycosphingolipids are required for sorting melanosomal proteins in the Golgi complex. J Cell Biol. 2001; 155:369–380. [PubMed: 11673476]

28. Hirosaki K, Yamashita T, Wada I, Jin HY, Jimbow K. Tyrosinase and tyrosinase-related protein 1 require Rab7 for their intracellular transport. J Invest Dermatol. 2002; 119:475–480. [PubMed: 12190873]

29. Gomez PF, Luo D, Hirosaki K, Shinoda K, Yamashita T, Suzuki J, Otsu K, Ishikawa K, Jimbow K. Identification of rab7 as a melanosome-associated protein involved in the intracellular transport of Tyrosinase-Related Protein 1. J Invest Dermatol. 2001; 117:81–90. [PubMed: 11442753]

30. Takechi Y, Hara I, Naftzger C, Xu Y, Houghton AN. A melanosomal membrane protein is a cell surface target for melanoma therapy. Clin Cancer Res. 1996; 2:1837–1842. [PubMed: 9816138]

31. Bennett DC, Cooper PJ, Hart IR. A line of non-tumorigenic mouse melanocytes, syngeneic with the B16 melanoma and requiring a tumour promoter for growth. Int J Cancer. 1987; 39:414–418. [PubMed: 3102392]

32. Prekeris R, Klumperman J, Chen YA, Scheller RH. Syntaxin 13 mediates cycling of plasma membrane proteins via tubulovesicular recycling endosomes. J Cell Biol. 1998; 143:957–971. [PubMed: 9817754]

33. Maxfield FR, McGraw TE. Endocytic recycling. Nature Rev Mol Cell Biol. 2004; 5:121–132. [PubMed: 15040445]
34. Kobayashi T, Stang E, Fang KS, de Moerloose P, Parton RG, Gruenberg J. A lipid associated with the antiphospholipid syndrome regulates endosome structure and function. Nature. 1998; 392:193–197. [PubMed: 9515966]
35. Kobayashi T, Beuchat MH, Chevallier J, Makino A, Mayran N, Escola JM, Lebrand C, Cosson P, Kobayashi T, Gruenberg J. Separation and characterization of late endosomal membrane domains. J Biol Chem. 2002; 277:32157–32164. [PubMed: 12065580]
36. White IJ, Bailey LM, Aghakhani MR, Moss SE, Futter CE. EGF stimulates annexin 1-dependent inward vesiculation in a multivesicular endosome subpopulation. EMBO J. 2006; 25:1–12. [PubMed: 16052208]
37. Peden AA, Oorschot V, Hesser BA, Austin CD, Scheller RH, Klumperman J. Localization of the AP-3 adaptor complex defines a novel endosomal exit site for lysosomal membrane proteins. J Cell Biol. 2004; 164:1065–1076. [PubMed: 15051738]
38. Lippincott-Schwartz J, Yuan LC, Bonifacino JS, Klausner RD. Rapid redistribution of Golgi proteins into the ER in cells treated with brefeldin A: evidence for membrane cycling from Golgi to ER. Cell. 1989; 56:801–813. [PubMed: 2647301]
39. Doms RW, Russ G, Yewdell JW. Brefeldin A redistributes resident and itinerant Golgi proteins to the endoplasmic reticulum. J Cell Biol. 1989; 109:61–72. [PubMed: 2745557]
40. van Dam EM, Stoorvogel W. Dynamin dependent transferrin receptor recycling by endosome-derived clathrin-coated vesicles. Mol Biol Cell. 2002; 13:169–182. [PubMed: 11809831]
41. Futter CE, Gibson A, Allchin EH, Maxwell S, Ruddock LJ, Odorizzi G, Domingo D, Trowbridge IS, Hopkins CR. In polarized MDCK cells basolateral vesicles arise from clathrin-gamma-adaptin-coated domains on endosomal tubules. J Cell Biol. 1998; 141:611–623. [PubMed: 9566963]
42. Chin LS, Raynor MC, Wei X, Chen HQ, Li L. Hrs interacts with sorting nexin 1 and regulates degradation of epidermal growth factor receptor. J Biol Chem. 2001; 276:7069–7078. [PubMed: 11110793]
43. Komada M, Masaki R, Yamamoto A, Kitamura N. Hrs, a tyrosine kinase substrate with a conserved double zinc finger domain, is localized to the cytoplasmic surface of early endosomes. J Biol Chem. 1997; 272:20538–20544. [PubMed: 9252367]
44. Urbé S, Sachse M, Row PE, Preisinger C, Barr FA, Strous GJ, Klumperman J, Clague MJ. The UIM domain of Hrs couples receptor sorting to vesicle formation. J Cell Sci. 2003; 116:4169–4179. [PubMed: 12953068]
45. Scoles DR, Qin Y, Nguyen V, Gutmann DH, Pulst SM. HRS inhibits EGF receptor signaling in the RT4 rat schwannoma cell line. Biochem Biophys Res Comm. 2005; 335:385–392. [PubMed: 16083858]
46. Hislop JN, Marley A, Von Zastrow M. Role of mammalian vacuolar protein-sorting proteins in endocytic trafficking of a non-ubiquitinated G protein-coupled receptor to lysosomes. J Biol Chem. 2004; 279:22522–22531. [PubMed: 15024011]
47. Raiborg C, Bremnes B, Mehlum A, Gillooly DJ, D'Arrigo A, Stang E, Stenmark H. FYVE and coiled-coil domains determine the specific localisation of Hrs to early endosomes. J Cell Sci. 2001; 114:2255–2263. [PubMed: 11493665]
48. Stenmark H, Parton RG, Steele-Mortimer O, Lutcke A, Gruenberg J, Zerial M. Inhibition of rab5 GTPase activity stimulates membrane fusion in endocytosis. EMBO J. 1994; 13:1287–1296. [PubMed: 8137813]
49. Prekeris R, Yang B, Oorschot V, Klumperman J, Scheller RH. Differential roles of syntaxin 7 and syntaxin 8 in endosomal trafficking. Mol Biol Cell. 1999; 10:3891–3908. [PubMed: 10564279]
50. Mullock BM, Smith CW, Ihrke G, Bright NA, Lindsay M, Parkinson EJ, Brooks DA, Parton RG, James DE, Luzio JP, Piper RC. Syntaxin 7 is localized to late endosome compartments, associates with Vamp 8, and Is required for late endosome-lysosome fusion. Mol Biol Cell. 2000; 11:3137–3153. [PubMed: 10982406]
51. Clague MJ, Urbe S. Hrs function: viruses provide the clue. Trends Cell Biol. 2003; 13:603–606. [PubMed: 14624836]

52. Raiborg C, Stenmark H. Hrs and endocytic sorting of ubiquitinated membrane proteins. Cell Struct Funct. 2002; 27:403–408. [PubMed: 12576633]
53. Bache KG, Brech A, Mehlum A, Stenmark H. Hrs regulates multivesicular body formation via ESCRT recruitment to endosomes. J Cell Biol. 2003; 162:435–442. [PubMed: 12900395]
54. Razi M, Futter CE. Distinct roles for Tsg101 and Hrs in multivesicular body formation and inward vesiculation. Mol Biol Cell. 2006; 17:3469–3483. [PubMed: 16707569]
55. Komada M, Soriano P. Hrs, a FYVE finger protein localized to early endosomes, is implicated in vesicular traffic and required for ventral folding morphogenesis. Genes & Dev. 1999; 13:1475–1485. [PubMed: 10364163]
56. Lloyd TE, Atkinson R, Wu MN, Zhou Y, Pennetta G, Bellen HJ. Hrs regulates endosome membrane invagination and tyrosine kinase receptor signaling in Drosophila. Cell. 2002; 108:261–269. [PubMed: 11832215]
57. Bilodeau PS, Winistorfer SC, Kearney WR, Robertson AD, Piper RC. Vps27-Hse1 and ESCRT-I complexes cooperate to increase efficiency of sorting ubiquitinated proteins at the endosome. J Cell Biol. 2003; 163:237–243. [PubMed: 14581452]
58. Lu Q, Hope LW, Brasch M, Reinhard C, Cohen SN. TSG101 interaction with HRS mediates endosomal trafficking and receptor down-regulation. Proc Natl Acad Sci USA. 2003; 100:7626–7631. [PubMed: 12802020]
59. Pornillos O, Higginson DS, Stray KM, Fisher RD, Garrus JE, Payne M, He GP, Wang HE, Morham SG, Sundquist WI. HIV Gag mimics the Tsg101-recruiting activity of the human Hrs protein. J Cell Biol. 2003; 162:425–434. [PubMed: 12900394]
60. Katzmann DJ, Stefan CJ, Babst M, Emr SD. Vps27 recruits ESCRT machinery to endosomes during MVB sorting. J Cell Biol. 2003; 162:413–423. [PubMed: 12900393]
61. Filimonenko M, Stuffers S, Raiborg C, Yamamoto A, Malerød L, Fisher EMC, Isaacs A, Brech A, Stenmark H, Simonsen A. Functional multivesicular bodies are required for autophagic clearance of protein aggregates associated with neurodegenerative disease. J Cell Biol. 2007; 179:485–500. [PubMed: 17984323]
62. Rusten TE, Vaccari T, Lindmo K, Rodahl LMW, Nezis IP, Sem-Jacobsen C, Wendler F, Vincent JP, Brech A, Bilder D, Stenmark H. ESCRTs and Fab1 regulate distinct steps of autophagy. Curr Biol. 2007; 17:1817–1825. [PubMed: 17935992]
63. Lee JA, Beigneux A, Ahmad ST, Young SG, Gao FB. ESCRT-III dysfunction causes autophagosome accumulation and neurodegeneration. Curr Biol. 2007; 17:1561–1567. [PubMed: 17683935]
64. Morita E, Sandrin V, Chung HY, Morham SG, Gygi SP, Rodesch CK, Sundquist WI. Human ESCRT and ALIX proteins interact with proteins of the midbody and function in cytokinesis. EMBO J. 2007; 26:4215–5227. [PubMed: 17853893]
65. Carlton JG, Martin-Serrano J. Parallels between cytokinesis and retroviral budding: a role for the ESCRT machinery. Science. 2007; 316:1908–1912. [PubMed: 17556548]
66. Spitzer C, Schellmann S, Sabovljevic A, Shahriari M, Keshavaiah C, Bechtold N, Herzog M, Müller S, Hanisch FG, Hülskamp M. The Arabidopsis elch mutant reveals functions of an ESCRT component in cytokinesis. Development. 2006; 133:4679–4689. [PubMed: 17090720]
67. Bishop N, Woodman P. ATPase-defective mammalian VPS4 localizes to aberrant endosomes and impairs cholesterol trafficking. Mol Biol Cell. 2000; 11:227–239. [PubMed: 10637304]
68. Theos AC, Berson JF, Theos SC, Herman KE, Harper DC, Tenza D, Sviderskaya EV, Lamoreux ML, Bennett DC, Raposo G, Marks MS. Dual loss of ER export and endocytic signals with altered melanosome morphology in the *silver* mutation of Pmel17. Mol Biol Cell. 2006; 17:3598–3612. [PubMed: 16760433]
69. Berson JF, Harper D, Tenza D, Raposo G, Marks MS. Pmel17 initiates premelanosome morphogenesis within multivesicular bodies. Mol Biol Cell. 2001; 12:3451–3464. [PubMed: 11694580]
70. Berson JF, Theos AC, Harper DC, Tenza D, Raposo G, Marks MS. Proprotein convertase cleavage liberates a fibrillogenic fragment of a resident glycoprotein to initiate melanosome biogenesis. J Cell Biol. 2003; 161:521–533. [PubMed: 12732614]

71. Hoashi T, Watabe H, Muller J, Yamaguchi Y, Vieira WD, Hearing VJ. MART-1 is required for the function of the melanosomal matrix protein PMEL17/GP100 and the maturation of melanosomes. J Biol Chem. 2005; 280:14006–14016. [PubMed: 15695812]
72. Valencia JC, Watabe H, Chi A, Rouzaud F, Chen KG, Vieira WD, Takahashi K, Yamaguchi Y, Berens W, Nagashima K, Shabanowitz J, Hunt DF, Appella E, Hearing VJ. Sorting of Pmel17 to melanosomes through the plasma membrane by AP1 and AP2: evidence for the polarized nature of melanocytes. J Cell Sci. 2006; 119:1080–1091. [PubMed: 16492709]
73. Wasmeier C, Romao M, Plowright L, Bennett DC, Raposo G, Seabra MC. Rab38 an Rab32 control early post-Golgi trafficking of melanogenic enzymes. J Cell Biol. 2006; 175:271–281. [PubMed: 17043139]
74. Van Den Bossche K, Naeyaert JM, Lambert J. The quest for the mechanism of melanin transfer. Traffic. 2006; 7:769–778. [PubMed: 16787393]
75. Mukhopadhyay A, Funato K, Stahl PD. Rab7 regulates transport from early to late endocytic compartments in Xenopus oocytes. J Biol Chem. 1997; 272:13055–13059. [PubMed: 9148916]
76. Press B, Feng Y, Hoflack B, Wandinger-Ness A. Mutant rab7 causes the accumulation of cathepsin D and cation-independent mannose 6-phosphate receptor in an early endocytic compartment. J Cell Biol. 1998; 140:1075–1089. [PubMed: 9490721]
77. Rink J, Ghigo E, Kalaidzidis Y, Zerial M. Rab conversion as a mechanism of progression from early to late endosomes. Cell. 2005; 122:735–749. [PubMed: 16143105]
78. Jordens I, Westbroek W, Marsman M, Rocha N, Mommaas M, Huizing M, Lambert J, Naeyaert JM, Neefjes J. Rab7 and Rab27a control two motor protein activities involved in melanosomal transport. Pigment Cell Res. 2006; 19:412–423. [PubMed: 16965270]
79. Di Pietro SM, Dell'Angelica EC. The cell biology of Hermansky-Pudlak syndrome: recent advances. Traffic. 2005; 6:525–533. [PubMed: 15941404]
80. Gautam R, Novak EK, Tan J, Wakamatsu K, Ito S, Swank RT. Interaction of Hermansky-Pudlak syndrome genes in the regulation of lysosome-related organelles. Traffic. 2006; 7:779–792. [PubMed: 16787394]
81. Wei ML. Hermansky–Pudlak syndrome: a disease of protein trafficking and organelle function. Pigment Cell Res. 2006; 19:19–42. [PubMed: 16420244]
82. Luyet PP, Falguières T, Pons V, Pattnaik AK, Gruenberg J. The ESCRT-I subunit TSG101 controls endosome-to-cytosol release of viral RNA. Traffic. 2008; 9:2279–2290. [PubMed: 18817529]
83. Ganesan AK, Ho H, Bodemann B, Petersen S, Aruri J, Koshy S, Richardson Z, Le LQ, Krasieva T, Roth MG, Farmer P, White MA. Genome-wide siRNA-based functional genomics of pigmentation identifies novel genes and pathways that impact melanogenesis in human cells. PLoS Genet. 2008; 4:e1000298. [PubMed: 19057677]
84. Myromslien FD, Grøvdal LM, Raiborg C, Stenmark H, Madshus IH, Stang E. Both clathrin-positive and -negative coats are involved in endosomal sorting of the EGF receptor. Exp Cell Res. 2006; 312:3036–3048. [PubMed: 16859684]
85. Sachse M, Strous GJ, Klumperman J. ATPase-deficient hVPS4 impairs formation of internal endosomal vesicles and stabilizes bilayered clathrin coats on endosomal vacuoles. J Cell Sci. 2004; 117:1699–1708. [PubMed: 15075231]
86. Camus G, Segura-Morales C, Molle D, Lopez-Vergès S, Begon-Pescia C, Cazevieille C, Schu P, Bertrand E, Berlioz-Torrent C, Basyuk E. The clathrin adaptor complex AP-1 binds HIV-1 and MLV Gag and facilitates their budding. Mol Biol Cell. 2007; 18:3193–3203. [PubMed: 17538020]
87. Katzmann DJ, Odorizzi G, Emr SD. Receptor downregulation and multivesicular-body sorting. Nature Rev Mol Cell Biol. 2002; 3:893–905. [PubMed: 12461556]
88. Lee JA, Beigneux A, Ahmad ST, Young SG, Gao FB. ESCRT-III dysfunction causes autophagosome accumulation and neurodegeneration. Curr Biol. 2007; 17:1561–1567. [PubMed: 17683935]
89. Raiborg C, Bache KG, Gillooly DJ, Madshus IH, Stang E, Stenmark H. Hrs sorts ubiquitinated proteins into clathrin-coated microdomains of early endosomes. Nature Cell Biol. 2002; 4:394–398. [PubMed: 11988743]

90. Garrus JE, von Schwedler UK, Pornillos OW, Morham SG, Zavitz KH, Wang HE, Wettstein DA, Stray KM, Cote M, Rich RL, Myszka DG, Sundquist WI. Tsg101 and the vacuolar protein sorting pathway are essential for hiv-1 budding. Cell. 2001; 107:55–65. [PubMed: 11595185]

91. Raposo, G.; Kleijmeer, MJ.; Posthuma, G.; Slot, JW.; Geuze, HJ. Immunogold labeling of ultrathin cryosections: application in immunology. In: Herzenberg, LA.; Weir, D.; Herzenberg, LA.; Blackwell, C., editors. Handbook of Exp Immunol. 5th. Cambridge, MA: Blackwell Science, Inc.; 1997. p. 1-11.

92. Berson JF, Frank DW, Calvo PA, Bieler BM, Marks MS. A common temperature-sensitive allelic form of human tyrosinase is retained in the endoplasmic reticulum at the nonpermissive temperature. J Biol Chem. 2000; 275:12281–12289. [PubMed: 10766867]

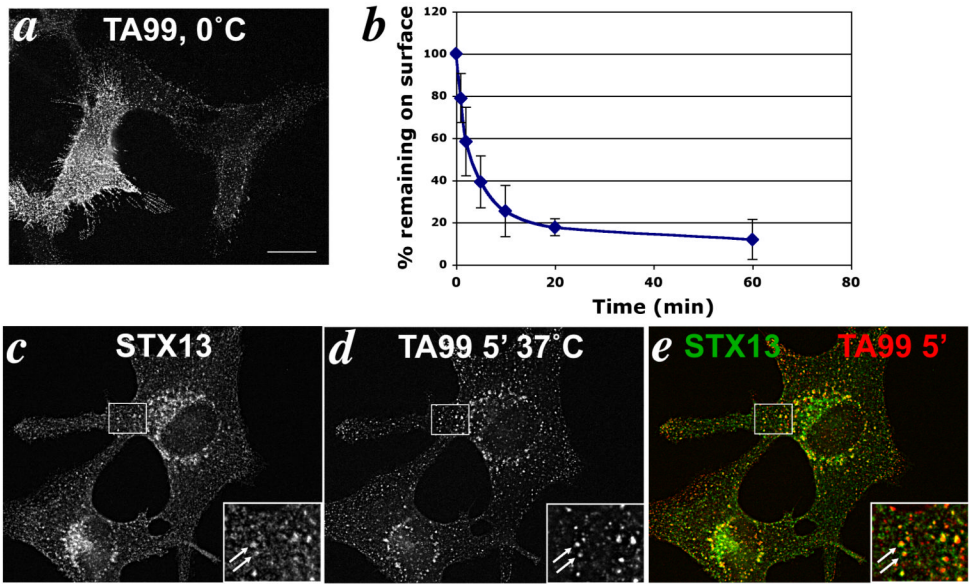

Figure 1. Tyrp1 at the cell surface is internalized into early endosomes

(*a*) Surface expression of Tyrp1. IFM analysis of melan-a cells incubated with TA99 antibody on ice, followed by fixation and staining with fluorophore-conjugated secondary antibody. Note that staining is not uniform across the surface but is localized to puncta within the membrane. (*b*) Tyrp1 endocytosis. Melan-a cells incubated with TA99 on ice were labeled with fluorophore-conjugated secondary antibody after the indicated times at 37°C, and then analyzed by flow cytometry. Mean fluorescence intensity values at each time point were normalized to that at time 0. Values represent mean +/- S.E.M. of three separate experiments each done in duplicate. (*e*) Internalized antibody localizes to early endosomes. IFM analysis of melan-a cells that had been bound to Alexa^{594}-conjugated TA99 antibody for 30 min on ice, and then internalized for 5 min at 37°C. Cells were labeled for syntaxin 13 (*c*) and analyzed directly for Alexa^{594} signal (*d*). Overlap of the two colorized images is shown in *e*. Insets, boxed areas shown at 2.5× magnification. Arrows mark areas of colocalization. Bar, 10 μm.

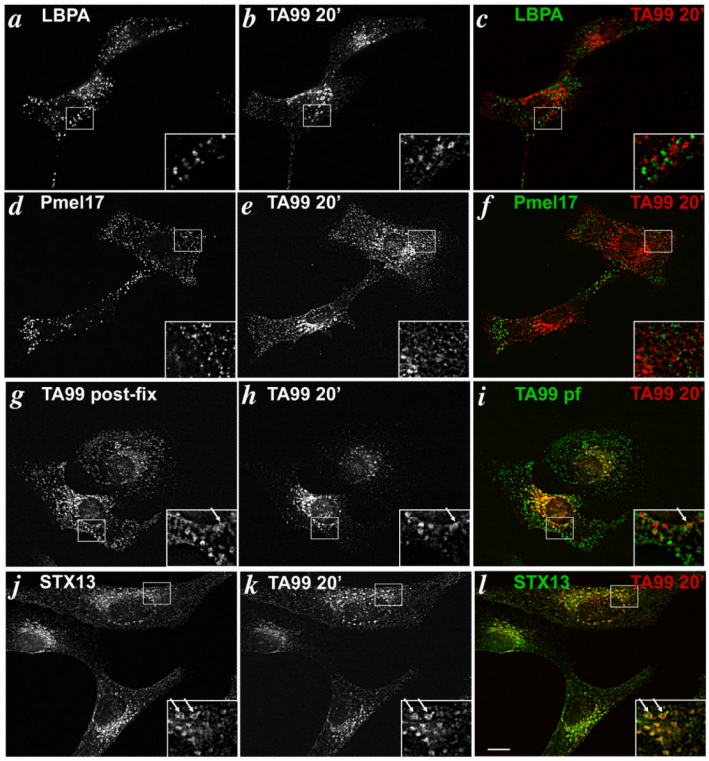

Figure 2. Cell surface Tyrp1 is inefficiently delivered to melanosomes after 20 min of chase

Melan-a cells that had internalized TA99-Alexa^{594} for 5 min were chased for 20 min in the absence of antibody, then fixed and labeled with primary antibodies to LBPA (*a-c*), Pmel17 (HMB45; *d-f*), TA99-Alexa^{488} (*g-i*), or syntaxin 13 (*j-l*), then with Alexa^{488}-conjugated secondary antibody. Cells were analyzed by IFM. Panels *c*,*f*,*i* and *l* represent merged, colorized images from the left two panels. Insets, boxed regions shown at 2.5× magnification. Arrows mark area of colocalization. Bar, 10 μm.

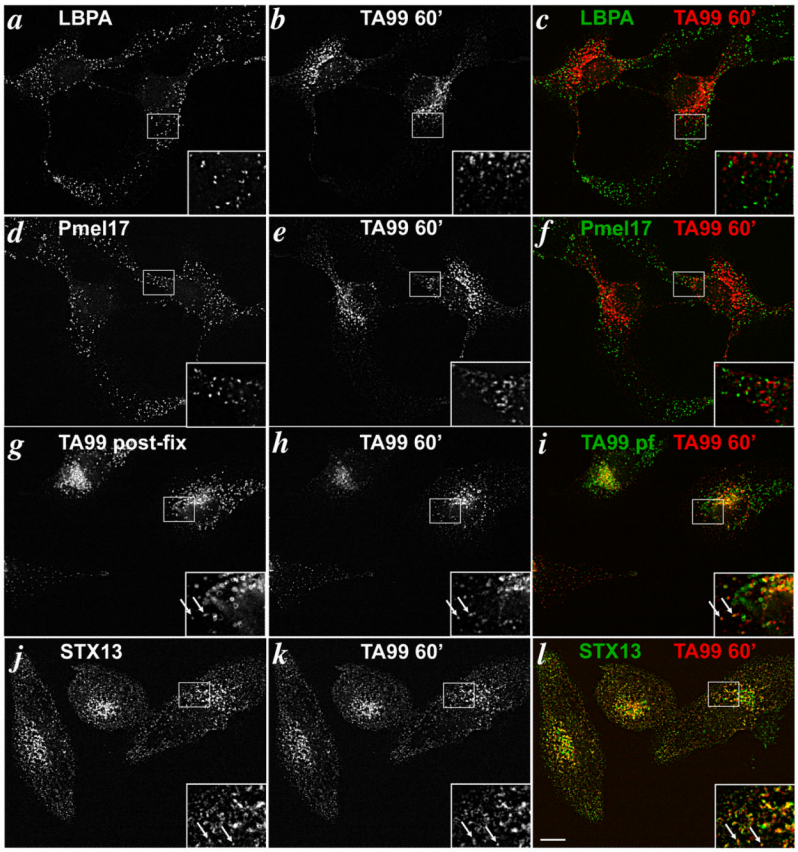

Figure 3. Cell surface Tyrp1 is delivered to melanosomes by 60 min chase

Same as Figure 4 except cells were analyzed after a 60 min chase in the absence of antibody. Legend is the same as in Figure 4.

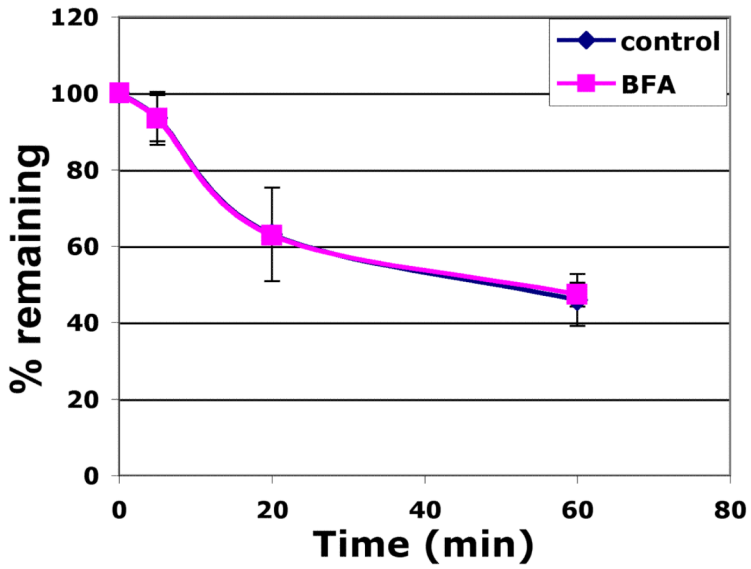

Figure 4. Cell surface Tyrp1 undergoes constitutive recycling

Melan-a cells that were untreated (blue line) or treated for 60 min with 10 μM BFA (pink line) were incubated with Alexa^{488}-conjugated TA99 on ice followed by incubation for 5 min at 37°C to internalize antibody/antigen complex in the absence or present of BFA. Cells were then incubated (+/- BFA) with anti-Alexa^{488} quenching antibody or a control non-quenching antibody for the indicated chase times. Remaining fluorescence was quantified by flow cytometry. Mean fluorescence intensity values for quenched samples were divided by values for non-quenched samples at each time point as a measure of % recycled antibody. Values represent mean +/- S.E.M. of three separate experiments each done in duplicate.

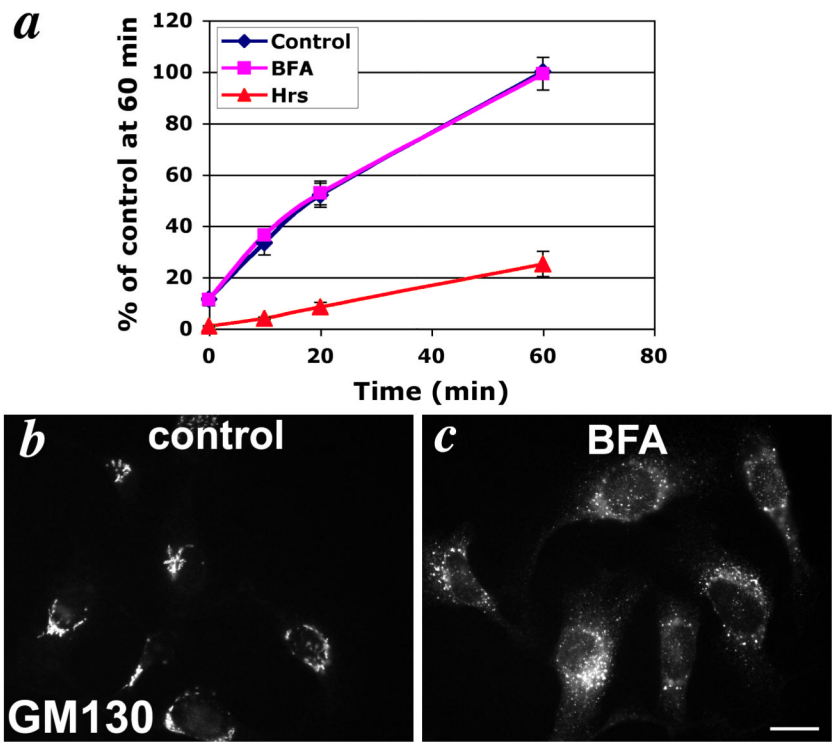

Figure 5. Tyrp1 is not biosynthetically delivered to the cell surface

(a) Continual antibody uptake assay. 1011-mel cells were incubated in the continuous presence of Alexa^{488}-conjugated TA99 antibody for the indicated time periods, and total cellular accumulation of Alexa^{488}-antibody was quantitated by flow cytometry. Cells were either untreated (blue line), treated with 10 μM BFA for 60 min prior to and during incubation with antibody (purple line), or transfected with 2 μg Hrs-myc and 0.2 μg EGFP-C3/ well 24-36 hrs earlier and gated for GFP expression during flow cytometric analysis (red line). Values represent the mean +/- S.E.M of mean fluorescence intensity values from three separate experiments, each done in duplicate, represented as a percentage of the mean fluorescence intensity value for control cells at 60 min. (*b*-*c*) IFM analysis of untreated (*b*, control) or BFA-treated (*c*, BFA) 1011-mel cells stained with anti GM130 antibody. Note the ribbon-like staining of the Golgi in control cells is completely dispersed in BFA-treated cells. Bar, 10 μm.

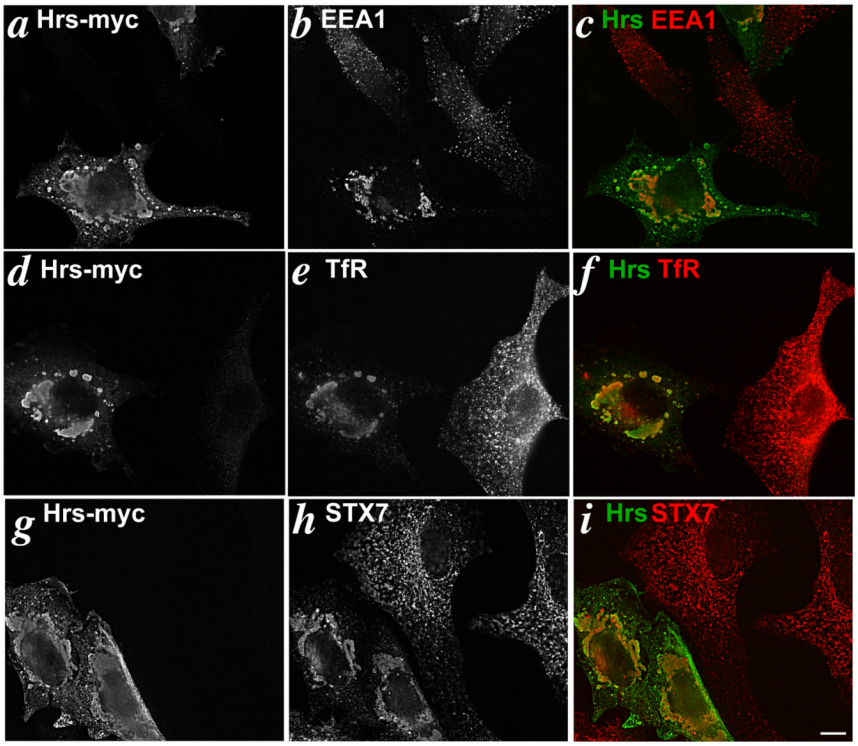

Figure 6. Hrs overexpression induces endosomal clustering

IFM analysis of 1011-mel cells transfected with 2 μg of Hrs-myc/well and fixed 24-36 hrs later. Cells were double labeled for the myc epitope tag and EEA1 (*a-c*), myc and TfR (*d-f*), or myc and syntaxin 7 (*g-i*). Panels *c*,*f* and *i* show overlap of the two images following colorization. Note the accumulation of Hrs-positive structures in the perinuclear region of a transfected cell in the same field as an untransfected cell. Bar, 10μm.

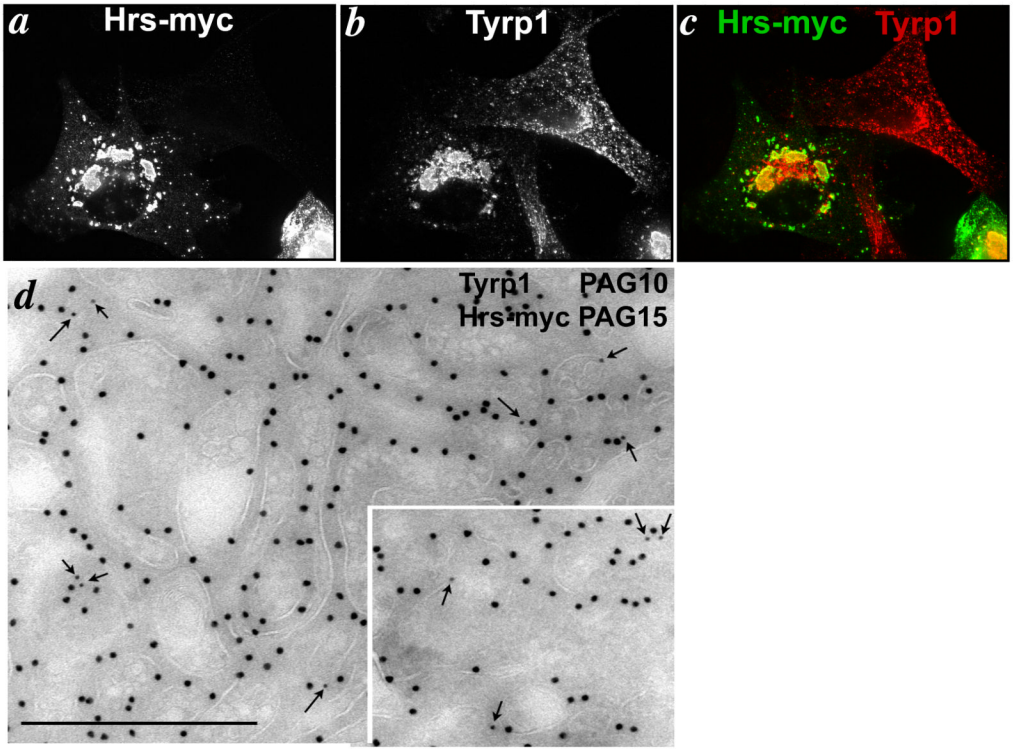

Figure 7. Tyrp1 is trapped in Hrs-positive compartments

1011-mel cells were transfected with 2 μg Hrs-myc/well and then fixed and analyzed 24-36 hours later by (*a*-*c*) IFM or (*d*) IEM. (*a*-*c*) Cells were double labeled for myc and Tyrp1. Panel c shows overlap of the two images following colorization. Note that Tyrp1 is redistributed to the Hrs-positive structures. Bar, 10 μm. (*d*) Cells were double immunogold labeled for Tyrp1 (PAG10) and Hrs (PAG15). Note the accumulation of label over the limiting membrane of clustered aberrant endosomal structures with weakly staining intralumenal membranes. Bar, 500 nm.

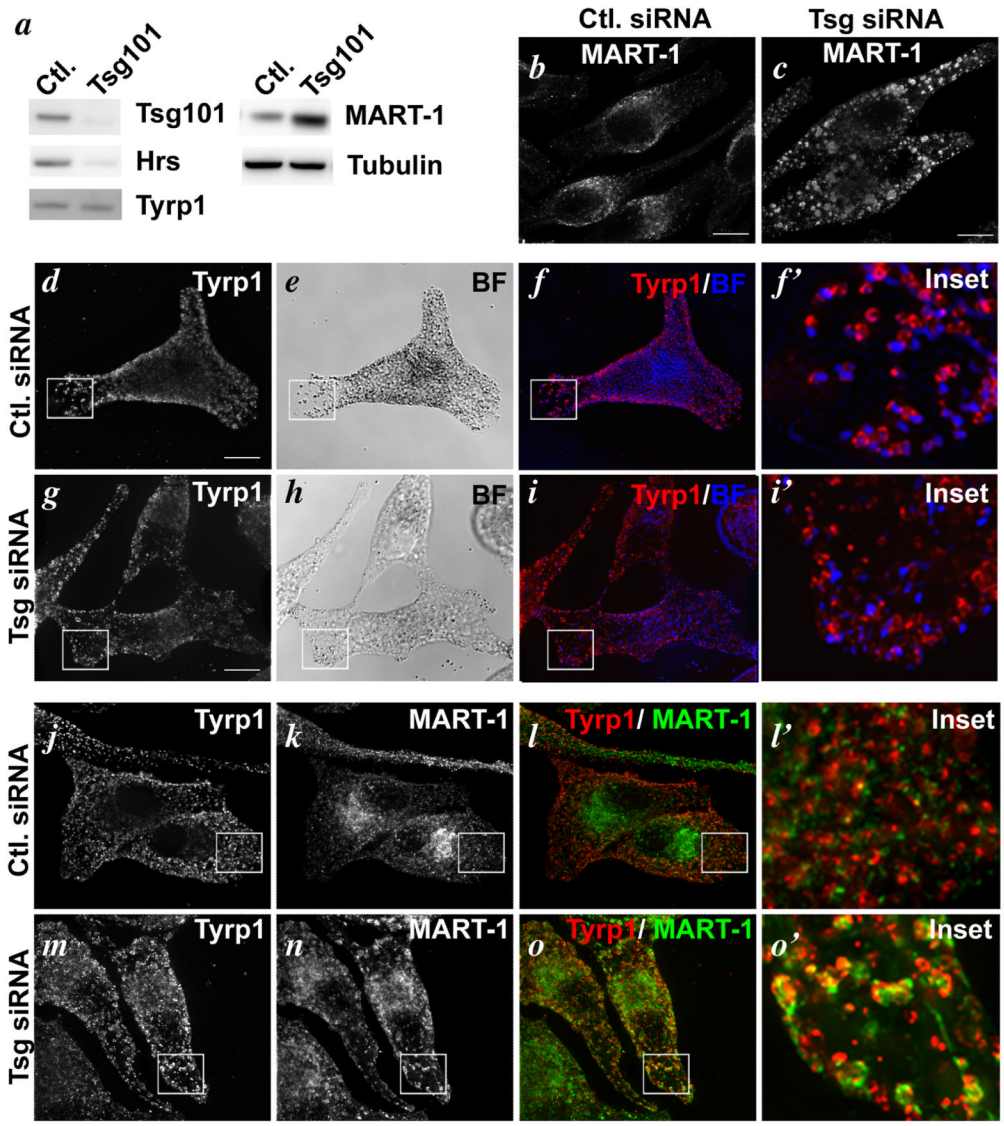

Figure 8. Missorting of Tyrp1 and MART-1 in cells depleted of Tsg101 by siRNA

MNT-1 cells were treated with control (Ctl.) siRNA or siRNA specific for Tsg101. *a.* Whole cell lysates from equal numbers of treated cells were fractionated by SDS-PAGE and analyzed by immunoblotting for endogenous Tsg101, Hrs, Tyrp1, MART-1, or tubulin as a control, as indicated. Note the depletion of Tsg101 and Hrs and the enrichment of MART-1 in cells treated with Tsg101 siRNA. *b-i.* Cells were analyzed by bright field microscopy (BF) or IFM using antibodies to MART-1 (*b*, *c*) or Tyrp1 (*d*, *f*, *f′ g*, *i*. *i′*) as indicated. Overlays (in which the pigment granules observed by bright field microscopy re pseudocolored blue) are shown in *f* and *i*; boxed regions are shown magnified 5× in *f′* and *i′*. *j-o.* Cells were analyzed by IFM using antibodies to Tyrp1 and MART-1 and isotype-specific secondary antibodies. Individual labels are shown in *j*, *k*, *m* and *n* and overlays are shown in *l* and *o*. *l′* and *o′* are 5× magnifications of the boxed regions shown in *l* and *o*. Bars, 10 μm.

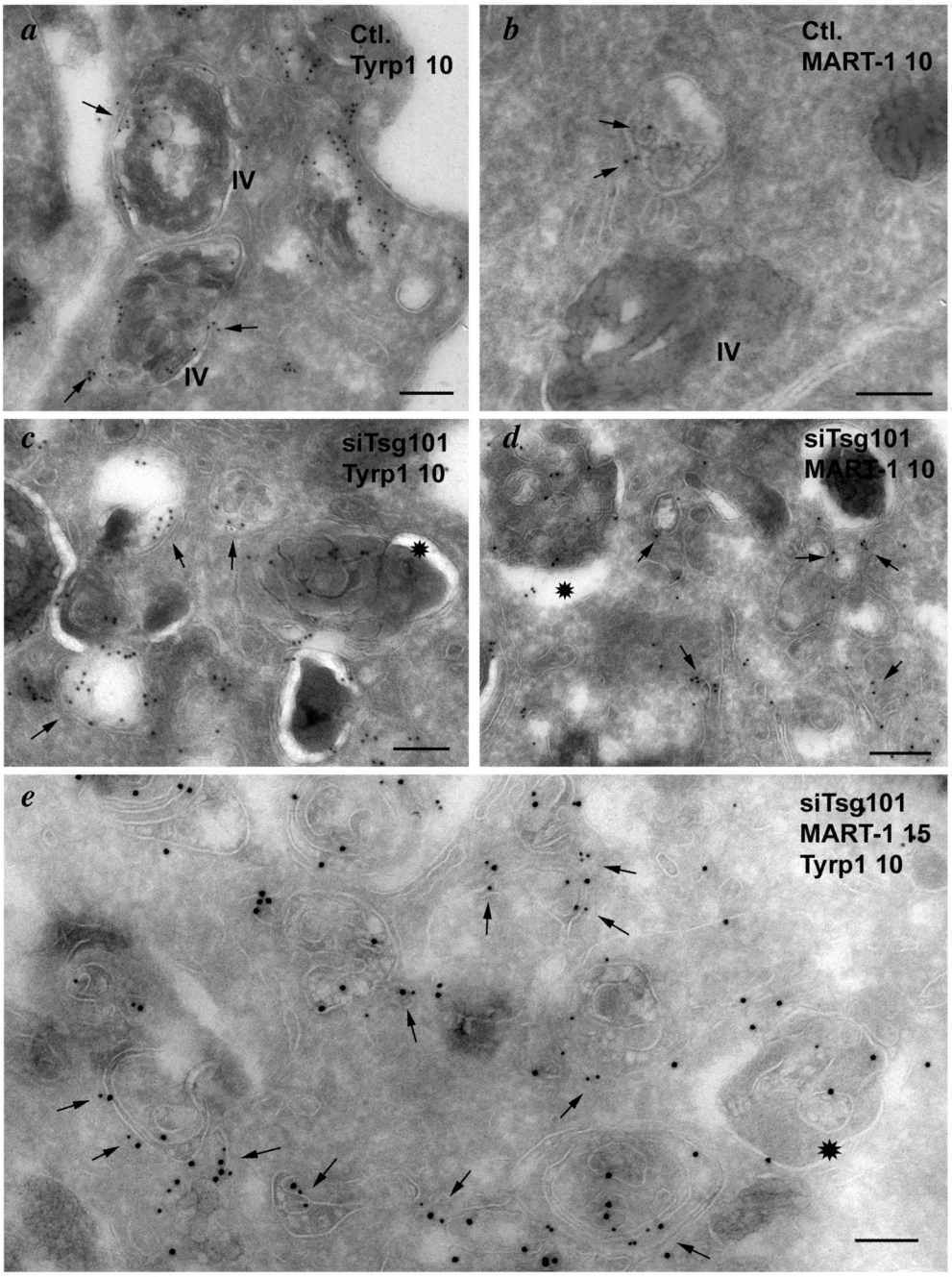

Figure 9. Tyrp1 and MART-1 localize to aberrant membranous structures in cells depleted of Tsg101 by siRNA

Ultrathin cryosections of MNT-1 cells treated with control (Ctl.; *a*, *b*) or Tsg101 siRNA (siTsg101; *c*-*e*) were immunogold labeled (PAG10) for Tyrp1 (*a*, *c*) or MART-1 (*b*, *d*) or double immunogold labeled for both (*e*; Tyrp1 PAG10, MART-1 PAG15) and analyzed by electron microscopy. Arrows in *a*-*d* point to representative labeling for each protein. Arrows in *e* point to examples of structures labeled with both antibodies. IV, stage IV melanosomes. Note the dense labeling for both Tyrp1 and MART-1 on aberrant structures with extensive internal membranes (*) in siTsg101 cells. Bars, 200 nm.

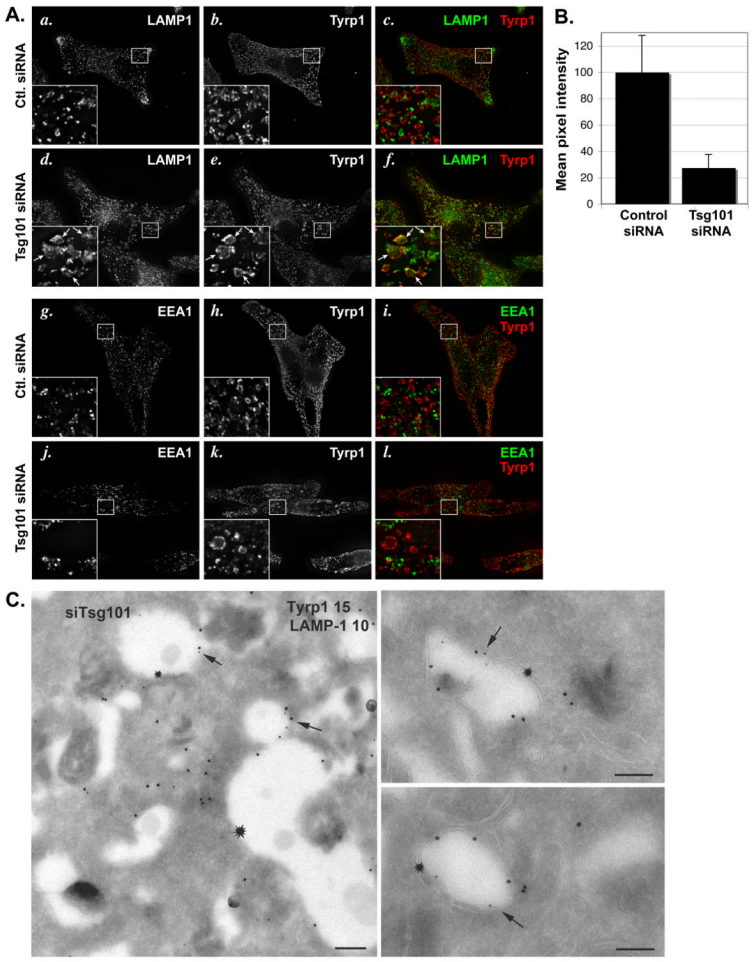

Figure 10. Tyrp1 codistributes with late endosomal markers and fails to recycle in cells depleted of Tsg101

MNT-1 cells were treated with control (Ctl.) or Tsg101 siRNA as indicated. *A.* Cells were analyzed by IFM using antibodies to Tyrp1 (*b*, *e*, *h*, *k*) and either LAMP1 (*a*, *d*) or EEA1 (*g*, *j*) as indicated and isotype-specific secondary antibodies; *c*, *f*, *i*, *l*, merged images. Insets show a 4× magnification of the boxed region. Arrows (*d*, *e*, *f*) denote enlarged vacuoles that label for both Tyrp1 and LAMP1. *Ba-c.* Ultrathin cryosections of cells transduced with siRNA to Tsg101 were double immunogold labeled for Tyrp1 (PAG15) and LAMP1 (PAG10) and analyzed by IEM. Note the vacuolar structures with a clear lumen in which the limiting membrane is labeled for both LAMP1 and Tyrp1 (arrows). In *a*, a small vacuole labeled for both markers emanates from a larger vacuole labeled only for Tyrp1 (asterisk). Bars, 500 nm. *C.* Cells were incubated for 60 min at 37°C with anti-Tyrp1 antibody, then fixed and processed for IFM using anti-MART-1 and isotype-specific secondary antibodies. Labeling for internalized anti-Tyrp1 antibody was quantified in at least 50 random control and Tsg101-depleted cells (the latter interpreted as cells treated with Tsg101 siRNA that expressed high levels of MART-1), and the mean pixel intensity value per cell was calculated and normalized to 100% for the control cell. The weighted mean and standard deviation calculated from the pooled variance of two separate experiments is shown.

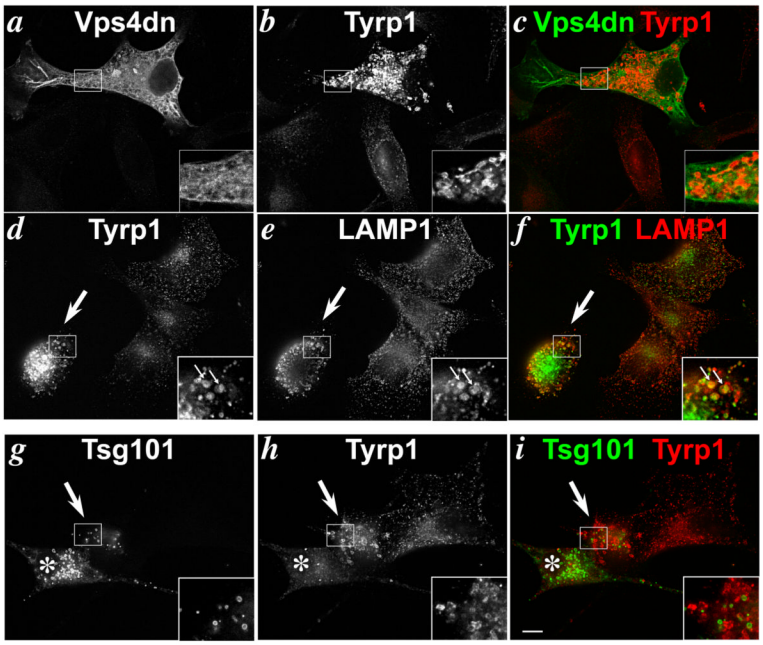

Figure 11. Tyrp1 delivery to melanosomes is blocked by dominant negative inhibition of ESCRT function

IFM analysis of 1011-mel cells transfected 24-36 hrs earlier with V5 epitope–tagged dnVps4 (*a-f*) or HA epitope-tagged Tsg101 (*g-i*) and costained with anti V5 and TA99 anti-Tyrp1 (*b,d,h*). Panels *c,f* and *i*, colorized and merged panels. Large arrow in *d-f* indicates a cell overexpressing dnVps4 as determined by triple labeling with goat-anti V5 antibody and detected by AMCA-conjugated anti-goat IgG (data not shown). Large arrow and star (*) in *g-i* indicate cells expressing modest and high levels of Tsg101, respectively. Insets are 2.5× magnification of boxed regions. Small arrows mark areas of colocalization. Bar, 10 μm.